Mon. Not. R. Astron. Soc. **000**, 1–34 (2014) Printed 28 May 2014 (MN LATEX style file v2.2)

UV spectral analysis of very hot H-deficient [WCE]-type central stars of planetary nebulae: NGC 2867, NGC 5189, NGC 6905, Pb 6, and Sand 3

Graziela R. Keller[1,2⋆], Luciana Bianchi[2] and Walter J. Maciel[1]

[1] *Instituto de Astronomia, Geofísica e Ciências Atmosféricas, Universidade de São Paulo, Cidade Universitária, São Paulo/SP, Brazil.*

[2] *Department of Physics and Astronomy, The Johns Hopkins University, 3400 N. Charles Street, Baltimore, MD 21218, USA.*

Released 2014 Xxxxx XX

ABSTRACT

We analysed UV FUSE, IUE, and HST/STIS spectra of five of the hottest [WCE]-type central stars of planetary nebulae: NGC 2867, NGC 5189, NGC 6905, Pb 6, and Sand 3. The analysis leveraged on our grid of CMFGEN synthetic spectra, which covers the parameter regime of hydrogen deficient central stars of planetary nebulae and allows a uniform and systematic study of the stellar spectra. The stellar atmosphere models calculated by us include many elements and ionic species neglected in previous analyses, which allowed us to improve the fits to the observed spectra considerably and provided an additional diagnostic line: the Ne VII λ 973 Å, which had not been modelled in [WCE] spectra and which presents, in these stars, a strong P-Cygni profile.

We report newly derived photospheric and wind parameters and elemental abundances. The central stars of NGC 2867, NGC 5189, and Pb 6 had their temperatures revised upward in comparison with previous investigations and we found the carbon to helium mass ratio of the sample objects to span a wide range of values, $0.42 < C : He < 1.96$. Modelling of the Ne VII λ 973 Å P-Cygni profile indicated strong neon overabundances for the central stars of NGC 2867, NGC 5189, NGC 6905, and Pb 6, with Ne mass fractions between 0.01 and 0.04. Nitrogen abundances derived by us for the central stars of NGC 5189, Pb 6, and Sand 3 are higher than previous determinations by factors of 3, 10, and 14, respectively.

Key words: stars: post-AGB – stars: atmospheres – stars: mass-loss – stars:

winds – stars: individual: NGC 2867 – stars: individual: NGC 5189 – stars: individual: NGC 6905 – stars: individual: Pb 6 – stars: individual: Sand 3

1 INTRODUCTION

Central stars of planetary nebulae, or CSPNe, are evolved stages of low- and intermediate-mass stars. They are very hot, with surface temperatures between 20,000 and 200,000 K, and many of them present signatures of strong stellar winds in their spectra. It is generally believed that the mass loss observed in these stars is driven by radiation pressure in spectral lines, the same mechanism thought to accelerate the winds of hot massive stars and which is intrinsically unstable and leads to the formation of density inhomogeneities usually called clumps (see, for example, Moffat 2008; Dessart and Owocki 2002, 2003, 2005; Oskinova et al. 2007; Sundqvist and Owocki 2013).

CSPNe are the connection between the asymptotic giant branch (AGB) phase and the white dwarfs (WDs) and are a unique opportunity to test stellar atmosphere, structure and evolution models. Their winds have the potential to impact subsequent stellar evolution and shape the planetary nebulae, which also owe their ionization to the strong radiation fields of the central stars. Thus, solid determinations of the photospheric and wind parameters of CSPNe, as well as of their chemical abundances, can help answering questions concerning stellar evolution, in particular the connection among the different types of hydrogen deficient central stars, the wind driving mechanism, and the surrounding nebulae.

It is estimated that about 30 per cent of CSPNe are hydrogen deficient (Weidmann and Gamen 2011). The main constituents of their atmospheres are, most commonly, helium, carbon, oxygen, neon, and, often, also nitrogen. Among the hydrogen deficient CSPNe, those evolving away from the AGB towards higher temperatures (in the Hertzsprung-Russell diagram - HRD), showing strong carbon and helium emission lines in their spectra, similar to massive Wolf-Rayet stars, are named [WC] stars, which are further divided into early ([WCE]) and late types ([WCL]), according to the ionization stages visible in their spectra. The hydrogen deficient CSPNe positioned at the top of the white dwarf cooling track in the HRD, exhibiting weak, or no wind features, in addition to absorption lines of highly ionized helium, carbon, and oxygen, belong to the PG1159 class. Due to the proximity of these types of hydrogen deficient CSPNe in the $\log T_* - \log g$ diagram and also because of

⋆ E-mail: graziela.keller@iag.usp.br, visiting scientist at JHU Department of Physics and Astronomy.

similarities in their abundance patterns, they are thought to form an evolutionary sequence, in which they would move away from the AGB and progress as [WC] stars towards higher temperatures, evolving from [WCL] to [WCE] types as their temperatures increase, until nuclear burning ceases and they enter the white dwarf cooling track. Their luminosities and mass-loss rates decrease and their winds reach the very high terminal velocities (up to 4000 km s^{-1}) typical of [WC]-PG1159 and PG1159 stars (Werner and Heber 1991; Górny and Tylenda 2000; Peña et al. 2001). Other classes of H-deficient post-AGB objects exist, which will not be discussed here (see, for example, Marcolino et al. 2007a; Todt et al. 2010, 2013; Rauch et al. 1998).

He, C, O, and Ne abundances observed in [WC] and PG1159 stars - which, however, vary greatly from one object to the other - resemble those of the intershell region of AGB models. According to Werner et al. (2007), in the case of PG1159 stars, the observed abundance intervals are: $X_{He} = 0.30 - 0.85$, $X_C = 0.15 - 0.60$, and $X_O = 0.02 - 0.20$. Abundance determinations for [WC] stars are approximately in the intervals: $X_{He} = 0.40 - 0.79$, $X_C = 0.15 - 0.55$, and $X_O = 0.01 - 0.15$ (Leuenhagen et al. 1996; Koesterke and Hamann 1997a,b; Leuenhagen and Hamann 1998; Koesterke et al. 1998; Marcolino et al. 2007b). Post-AGB evolutionary models are able to predict the helium, carbon, and oxygen abundance patterns seen in PG1159 and [WC] stars, explaining the wide range of values seen by differences in the initial mass of the stars and on the number of thermal pulses suffered during the AGB phase (see, for example, Werner et al. 2007, and references therein). Their hydrogen deficiency is usually thought to be the result of late thermal pulses, which can occur either at the tip of the AGB (in which case it is named an AGB final thermal pulse or AFTP), or during the post-AGB evolutionary phase, as in the very late thermal pulses (VLTP) of the born-again scenario of Iben et al. (1983) (taking place after the star has entered the WD cooling track in the HRD), or in the so called late thermal pulses (LTP) occurring during the CSPN phase (see Blöcker 2001; Herwig 2001; Althaus et al. 2005). Each of these scenarios produces H-deficient stars. However, the surface abundance patterns originated will differ between the scenarios (see, for example, Werner and Herwig 2006, and references therein).

[WCE] CSPNe are thus the hottest among [WC]-type stars and are probably the direct predecessors of [WC]-PG1159 and PG1159 stars, which are, in turn, believed to evolve into DA and DO WDs (Althaus et al. 2010). Their analysis can help establish constraints for the different post-AGB evolutionary scenarios. The spectra shown by the hottest [WCE] stars are characterized by lack of photospheric absorption lines, the presence of strong, broad

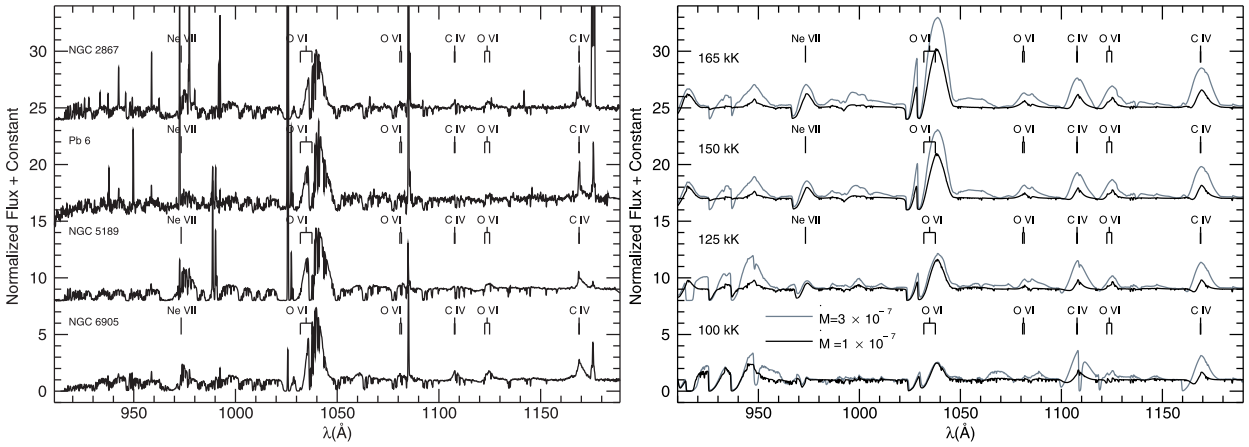

Figure 1. Left panel: FUSE spectra of the [WCE] CSPNe NGC 6905, NGC 5189, Pb 6 and NGC 2867. The numerous narrow absorptions are due to interstellar H_2, which affects the blue edge of the Ne VII P-Cygni profile. Right panel: sample synthetic spectra from our model grid, calculated for different values of stellar temperature and two different mass-loss rates (in units of $M_\odot$ yr^{-1}). All models shown adopt $v_\infty = 2500$ km s^{-1} and models of the same temperature adopt the same stellar radius. The observed and synthetic spectra shown were convolved with a Gaussian of 0.2 Å FWHM for clarity.

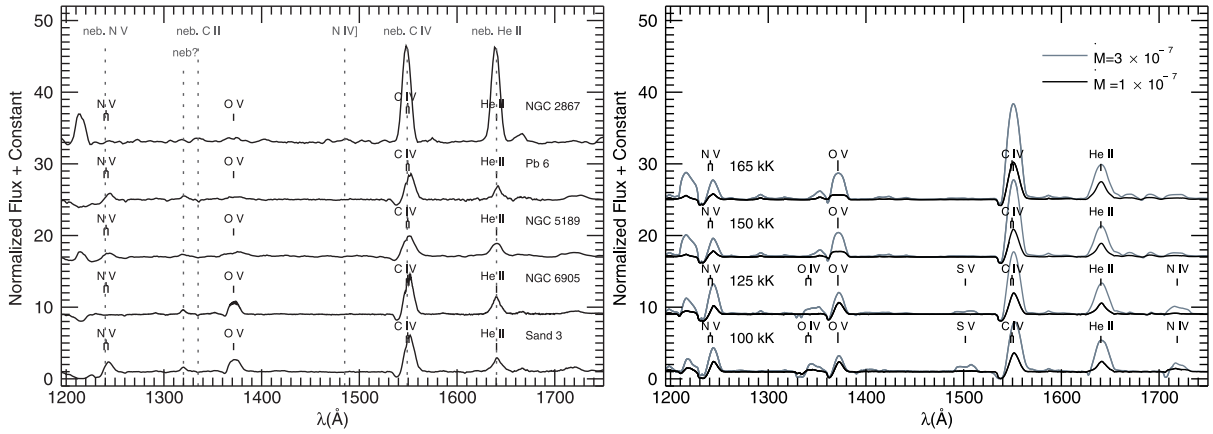

Figure 2. Left panel: HST/STIS G140L spectra of the [WCE] CSPNe NGC 6905, Pb 6 and Sand 3, and low resolution IUE spectra of NGC 5189 and NGC 2867. The dotted vertical lines indicate the location of emission lines commonly seen in PNe. Feibelman (1996b) identified the structure around 1320 Å as being a nebular [Mg V] line in the spectra of Sand 3. We, however, find evidence of its stellar origin, as we discuss on Section 2. Right panel: sample synthetic spectra from our model grid (same models as in Fig. 1), between 1200 and 1750 Å, calculated for different values of stellar temperature and two different mass-loss rates (in units of $M_\odot$ yr^{-1}). The synthetic spectra shown were convolved with a HST/STIS G140L instrumental LSF.

emission lines, UV P-Cygni profiles, and a paucity of lines in the optical region, in which none of the few strong lines they present have P-Cygni profiles. Essential diagnostic lines lay shortwards of Ly α, in the far-UV range, which was provided by FUSE (Far Ultraviolet Spectroscopic Explorer - 905−1187 Å - Moos et al. (2000)). In this region, these stars show two conspicuous P-Cygni profiles: Ne VII λ 973.3 Å and O VI $\lambda\lambda$ 1031.9, 1037.6 Å, as shown in Fig. 1. Complementary line diagnostics are found in the spectral region between 1150 and 3200 Å, covered by IUE (International Ultraviolet Explorer) and HST (Hubble Space Telescope) spectrographs (Fig. 2). A detailed description of the UV spectra of [WCE] CSPNe was provided by Keller et al. (2011).

In this paper, we present a comparative analysis of UV and far-UV spectra of the hot [WCE]-type CSPNe NGC 2867, NGC 5189, NGC 6905, Pb 6, and Sand 3 (WO1 stars in the unified classification scheme of Crowther et al. (1998)), prompted by the lack of a comprehensive, systematic analysis of [WCE] CSPNe making use of the available high resolution spectra and of today's modern stellar atmosphere codes. Our analysis includes many ionic species neglected in previous works, thus allowing us to model, for the first time in [WCE] stars, the Ne far-UV spectral lines, besides improving the overall match between model and observations. The analysis was based on our extensive grid of synthetic spectra (Keller et al. 2011) and numerous subsequent model calculations for each individual object. A detailed analysis of the central star of NGC 6905 was presented in Keller et al. (2011) and the results are now compared with those obtained for the other stars studied in this work, placing the central star of NGC 6905 in the context of [WCE] CSPNe. With the exception of Pb 6, all CSPNe studied here are classified as GW Vir (=PG 1159−035) variables - a class of nonradial pulsating variable H-deficient pre-White Dwarfs, showing variability $\lesssim$0.3 mag (see Althaus et al. 2010, and references therein).

The paper is organized as follows: in Section 2, we describe the sample objects and the data used in the analysis. Section 3 describes the synthetic spectra. In Section 4, we describe the spectral analysis of the sample objects. Finally, we present our conclusions in Section 5.

2 SAMPLE OBJECTS AND DATA

The objects studied here, the central stars of NGC 2867, NGC 5189, NGC 6905, Pb 6, and Sand 3, belong to the small group of [WCE] stars for which good quality UV spectra exist: quality far-UV FUSE spectra exist for four of these stars (NGC 2867, NGC 5189, NGC 6905, and Pb 6). However, only for NGC 6905 and Pb 6 there are complementary HST/STIS UV spectra. In the case of NGC 5189 and NGC 2867, we used complementary IUE low resolution spectra. Sand 3, on the other hand, has excellent HST/STIS G140L and G230MB spectra, but no FUSE, which limits the available line diagnostics, but its analysis is nonetheless interesting, particularly for its spectral similarity to the other stars, especially to the central star of NGC 6905. The available STIS spectra of Sand 3 were complemented by low resolution IUE spectra between 1725 and 3300 Å.

Our sample objects are listed in Table 1, along with radial velocities (v_{rad}), distances, and nebular parameters (expansion velocity - v_{exp}, angular diameter, and shape). Throughout

Table 1. Sample objects.

Object	v_{rad} [km s$^-$1]	Dist. [kpc]	Nebular Diam. [arcsec]	v_{exp} [km s$^-$1]	Shape
NGC 6905	-8.4[a]	1.73[e]; 1.75[f]; 1.80[g]	43.3 × 35.6[d]	43.5[a]	Elliptical
NGC 5189	-9.2[a]	0.54[e]; 0.55[f]; 0.70[g]	163.4 × 108.2[d]	36.0[a]	Quadrupolar
Pb 6	56.0[b]	4.38[e]; 4.42[f]; 4.00[g]	5.5[e]	?	Unclassified
NGC 2867	14.4[b]	1.84[e]; 2.23[f]; 1.60[g]	14.4 × 13.9[d]	18.9[a]	Elliptical
Sand 3	-92.5[c]	?	–	–	No detectable nebulosity

[a]Acker et al. (1992); [b]Peña et al. (2013); [c]Feibelman (1996b); [d]Tylenda et al. (2003); [e]Cahn et al. (1992); [f]Stanghellini et al. (2008); [g]Maciel (1984).

this paper, the observed spectra presented in the figures have been shifted to the rest frame of the star, using the listed radial velocities. The utilized spectra are listed in Table 2. IUE, HST/STIS, and FUSE spectra used in the analysis were retrieved from MAST (Mikulski Archive for Space Telescopes - `http://archive.stsci.edu/`). NGC 2867, NGC 5189, and Pb 6 FUSE and Pb 6 and Sand 3 STIS spectra have not been used in stellar atmosphere modelling before this work. NGC 6905's STIS spectra, as well as the region of its FUSE spectra shortwards of 1000 Å, in which the strong P-Cygni profile of the λ 973.3 Å Ne VII line can be found, were first modelled by us and presented in Keller et al. (2011). The objects were thus selected among the known sample of hot [WCE] CSPNe for the availability of good UV spectra, most of them not previously analysed.

2.1 Description of the utilized data

2.1.1 FUSE data

The FUSE instrument included four channels (LiF1, LiF2, SiC1, SiC2), each divided into two segments (A and B), collecting light simultaneously. Each channel-segment combination spans a fraction of FUSE's nominal wavelength coverage, with some overlap among them. All FUSE spectra used in this work were obtained through the $30'' \times 30''$ aperture, in time-tag mode. We used the CalFUSE v3.2.2 pipeline for data reduction, along with the FUSE IDL tools 'CF_edit' and 'FUSE_register'. We screened the observations for bad time intervals, and checked for possible drifting of the target out of the aperture. The spectra of the different segments were then extracted with the 'cf_extract_spectra' routine. Faulty regions of the spectra, such as those close to the detectors' edges and the region of the LiF 1B detector affected by the artefact known as 'worm' (due to a shadow thrown on the detector by the instrument itself) were removed and the spectra of the different segments, co-added weighted by their errors.

In the case of CSPN Pb 6, continuum flux levels differ between FUSE and HST/STIS

Table 2. Spectral data sets analysed in this work.

Instrument	Data ID	Date	Resol. [Å]	Aperture ["]	Range [Å]	comments
NGC 6905						
FUSE	A1490202000	2000 Aug 11	∼0.06	30×30	905−1187	
STIS + G140L	O52R01020	1999 Jun 29	∼1.20	52×0.5	1150−1730	
STIS + G230L	O52R01010	1999 Jun 29	∼3.15	52×0.5	1570−3128	
NGC 5189						
FUSE	S6013001000	2002 Feb 28	∼0.06	30×30	905−1187	
IUE	LWR07171	1980 Mar 12	∼7.0	10×20	1850−3300	
IUE	SWP08219	1980 Mar 12	∼6.0	10×20	1150−2000	
IUE	SWP06327	1979 Aug 30	∼6.0	10×20	1150−2000	off star
IUE	LWR01985	1978 Aug 05	∼7.0	10×20	1850−3300	off star
IUE	SWP02206	1978 Aug 05	∼6.0	10×20	1150−2000	off star
IUE	SWP25365	1985 Mar 05	∼6.0	10×20	1150−2000	off star
IUE	LWP05456	1985 Mar 05	∼7.0	10×20	1850−3300	
IUE	LWP05457	1985 Mar 05	∼7.0	10×20	1850−3300	off star
IUE	SWP25363	1985 Mar 05	∼0.2	10×20	1150−2000	bad extraction
IUE	SWP25364	1985 Mar 05	∼6.0	10×20	1150−2000	
IUE	SWP41913	1991 Jun 24	∼6.0	10×20	1150−2000	off star
Pb 6						
FUSE	Z9111101000	2003 Feb 20	∼0.06	30×30	905−1187	
STIS + G140L	OBRZ23010	2012 Apr 25	∼1.20	52×0.2	1150−1730	
STIS + G230L	OBRZ23020	2012 Apr 25	∼3.15	52×0.2	1570−3180	
STIS + G230L	OBRZ23030	2012 Apr 25	∼3.15	52×0.2	1570−3180	
NGC 2867						
FUSE	Z9110901000	2003 Feb 22	∼0.06	30×30	905−1187	
IUE	SWP05234	1979 May 14	∼6.0	10×20	1150−2000	noisy
IUE	SWP05215	1979 May 12	∼6.0	10×20	1150−2000	
IUE	LWR04510	1979 May 12	∼7.0	10×20	1850−3300	
IUE	LWR04518	1979 May 14	∼7.0	10×20	1850−3300	
IUE	SWP08984	1980 May 12	∼0.2	10×20	1150−2000	bad extraction
IUE	SWP52948	1994 Nov 30	∼0.2	10×20	1150−2000	bad extraction
IUE	LWR07736	1980 May 12	∼0.2	10×20	1850−3300	bad extraction
Sand 3						
STIS + G140L	O4XH01030	1998 Sep 03	∼1.20	52×2	1138−1725	
STIS + G230MB	O4XH01020	1998 Sep 03	∼0.33	52×2	2716−2872	
IUE	SWP53882	1995 Feb 10	∼6.0	10×20	1150−1975	
IUE	LWR05765	1979 Oct 06	∼7.0	10×20	1860−3300	

SWP53882 is only used in the interval 1725−1851 Å.

spectra, with the former being 40 per cent higher. Such divergences in flux levels are often related to the positioning of the target into the instrument's aperture or difficulties in extracting the background in low signal-to-noise data. A comparison between HST G140L and IUE low resolution (SWP29857) spectra of Pb 6 shows agreement in continuum levels within 10 per cent. Flux levels also agree between G140L and G230L spectra of Pb 6. According to Bohlin and Hartig (1998), the STIS $52'' \times 0.2''$ aperture is calibrated to a few percent accuracy, with the repeatability for point sources being at worse 10 per cent, with a RMS of 4.5 per cent. We thus have scaled the flux level of the FUSE spectrum of Pb 6 down by dividing it by 1.4 to match that of the STIS spectrum.

The FUSE spectra of the central stars studied here present some strong and narrow emissions that do not seem to originate in the atmospheres of these stars, for they are much narrower than their typically broad wind lines. Some of these emissions are due to

the planetary nebulae and some are due to airglow or scattered sun light, as verified by comparing the spectra obtained during the orbital night with the composite of all data. Except for NGC 2867, for which the signal to noise ratio of the available FUSE spectra allowed us to use night only events, thus minimizing airglow contamination, both orbital night and day time-tag events were used in the stellar spectra of the sample objects.

The central stars of NGC 2867 and NGC 5189 have 3 FUSE observations each. We have used those with the highest signal-to-noise ratio. While the plot previews available at the MAST website show some variation of flux levels and line profiles between different data sets, the careful treatment of the data, as described above, aiming at mitigating the effects of channel drift, airglow, faulty centroid positioning, worms and dead zones, strongly diminishes the disagreements between the spectra obtained in different observations, which are now on the same level as those seen comparing spectra from the same observation, but from different channels, suggesting that instrumental effects plus others such as airglow (which can be minimized by the use of night only time-tag events, but is never completely absent) may be responsible for the remaining small variations in line profiles and flux levels.

2.1.2 IUE data

Despite the fact that MAST lists all IUE spectra for NGC 5189 under the category 70, which is described there as observation of nebula plus central star, our analysis of the spectra indicate that many of the exposures actually missed the central star, as in the case of SWP25363 - the only high resolution IUE spectrum available for NGC 5189. In the 2D high resolution SWP25363 spectral image, spatially extended nebular emission lines and only a very faint continuum are visible. The continuum is not centred, but at the edge of the illuminated region, which is evidence that flux was partially missed. The pipeline seems to have misplaced the extraction slit and part of the resulting net flux is below zero. Nonetheless, the spectral resolution of 0.2 Å allows us to estimate the width of the He II λ 1640.4 Å line as $\approx$0.6 Å, consistent with a nebular origin. We thus cannot establish from the echelle spectrum whether there is also stellar He II λ 1640.4 Å emission. Fig. 3 shows IUE SWP25364 and SWP25365 low-resolution spectra, which were taken at the same pointing coordinates and with the large aperture (10" $\times$ 20"), but at different position angles. The latter seems to have at least partially missed the central star. The difference between the two spectra exposes the nebular origin of the C III] λ 1909 Å line and indicates that at least

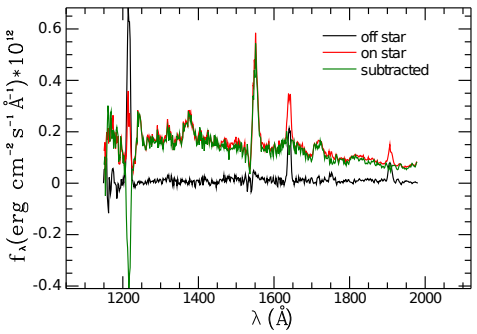

Figure 3. SWP25364 (red) and SWP25365 (black) low-resolution IUE spectra. The result of subtracting SWP25365 from SWP25364 is shown in green.

part of the He II λ 1640.4 Å emission seen in SWP25364 is of nebular origin. Therefore, we will regard NGC 5189's He II λ 1640.4 Å emission as an upper limit to the stellar line and leverage on other spectral lines to constrain the stellar parameters. Since there are no high-resolution spectra of NGC 5189's central star in the region between 1200 and 3200 Å, we rely on the low resolution data. For the present analysis of NGC 5189, we use SWP08219 and LWR07171, for being better centred and less noisy than the SWP25364 and LWP05456 spectra, respectively.

The available IUE low resolution spectra of NGC 2867 seem to be dominated by nebular emissions, such that P-Cygni profiles cannot be distinguished. The inspection of the spectral images of SWP05215 and LWR04510 shows well defined, well centred and narrow continua. Since only the strongest emission lines in the SWP05215 spectrum appear saturated and because its continuum has a higher signal than that of the noisy SWP05234 spectrum, we chose to show the former instead of the latter in this work, for it allows a more precise determination of the slope of the continuum, which will be used in the normalization of the observed spectra and to ascertain the colour excess. We will not use it for line strength analysis, except as an upper limit for stellar emission in some weaker lines. The existing high resolution IUE spectra of this star exhibit again very faint continua (in the two-dimensional spectra) and negative flux values (in the extracted spectra), indicating again extraction problems. No obvious stellar lines are apparent. Narrow and strong C IV $\lambda\lambda$ 1548.2, 1550.8 Å, He II λ 1640.4 Å and C III] λ 1909 Å nebular emission lines are, however, readily discernible in the high resolution spectra.

2.1.3 HST data

HST/STIS gratings are designed for spatially resolved spectroscopy using a long slit, exploiting HST's high spatial resolution capabilities. The HST/STIS spectra of CSPNe NGC 6905, Pb 6, and Sand 3 thus minimize nebular contamination of the stellar extracted spectra - in comparison with IUE spectra, for example. The inspection of the 2D G140L and G230L spectra of NGC 6905 and Pb 6 reveals extended nebular emission around ≈1909 (very faint in NGC 6905), 1550 and 1640 Å, as seen on the logarithmic scale plots in the supplementary figures, online. Other faint extended emissions are seen in the 2D G140L spectrum of Pb 6 around ≈1240, 1400 and 1485 Å. The 2D Sand 3 G140L spectrum does not exhibit evidence of nebular emissions, in line with the idea of its nebula having already dissipated (Barlow and Hummer 1982).

In neither 2D STIS spectra there is evidence of extended nebular emission close to the structure associated by Feibelman (1996b) with nebular [Mg V] $\lambda\lambda$ 1324.5 Å in the low resolution IUE spectra of Sand 3 and marked in Fig. 2, even though the extracted stellar spectra of all three objects observed with STIS show the feature, which, together with the evidence of Sand 3's nebula having dispersed, points towards a stellar origin for this spectral feature. Similarly, Feibelman (1996a) suggested the nebular He II λ 2253 Å and numerous [Ne V] lines between 2235 and 2265 Å seen in the high resolution IUE spectra of NGC 6905 as the sources of the wide emission feature seen in lower resolution spectra of this region. The origin of this spectral feature, however, seems to be at least partially stellar, since the strong feature appears not only in the low resolution IUE spectra of Sand 3 - despite its dispersed nebula not producing a detectable C III] λ 1909 Å emission - but also in the 1D STIS spectra of NGC 6905 and Pb 6, whose 2D G230L spectra do not show evidence of extended nebular emission in this region.

The agreement between the medium resolution (≈0.33 Å) HST/STIS G230MB observed spectrum of Sand 3's O V $\lambda\lambda$ 2781.0, 2787.0 Å line and the low resolution IUE spectrum of the same star indicates that this strong and wide line is from stellar origin. This was also verified from the inspection of the 2D G230MB spectrum of Sand 3 and of the 2D G230L spectra of NGC 6905 and Pb 6, which do not show extended emissions in this region.

3 MODELLING

3.1 Stellar models

The spectra of these very hot, H-poor CSPNe are dominated by broad, strong emission lines, which are signatures of their dense, high velocity stellar winds. Spectra of hot objects with detectable winds require modelling with non-LTE stellar atmosphere codes that account for expanding atmospheres. In this work, we used models computed with CMFGEN (Hillier and Miller 1998; Herald et al. 2005), which is a non-LTE, non-hydrodynamic code that considers a stationary mass loss in a spherically symmetric geometry, line blanketing (through the super-level approximation) and wind clumping (through the filling factor approach). The detailed workings of the code are described in the references above. The fundamental stellar parameters include stellar temperature (T_*) and radius (R_*), defined at an optical depth of τ =20, mass-loss rate ($\dot{M}$), terminal velocity of the wind (v_∞), velocity law, and elemental abundances. We assume a standard velocity law, $v(r) = v_\infty(1 - r_0/r)^\beta$, where $r_0 \approx R_*$ and $\beta = 1$, and an exponential law for the clumping filling factor (which is the fraction of the wind volume occupied by clumps), given by $f(v) = f_\infty + (1 - f_\infty) \exp(-v(r)/v_{clump})$, where v_{clump} = 200 km s^{-1} is the velocity beyond which the wind is no longer smooth and the clumping increases until the terminal value of $f_\infty = 0.1$ is reached.

The analysis leverages on the extensive grid of synthetic spectra computed by Keller et al. (2011), covering parameter values typical of H-poor CSPNe and approximately following the evolutionary tracks from Miller Bertolami and Althaus (2006). The grid allows for a uniform and systematic comparison of the spectral features and facilitates line identification and the determination of the main stellar parameters. The grid models adopt a constant abundance pattern: $X_C = 0.45$, $X_{He} = 0.43$, $X_O = 0.08$, $X_N = 0.01$, $X_{Ne} = 0.02$ in mass fractions, an iron abundance a factor of 100 lower than the solar value, and solar abundances for all other elements included into the calculations. Within the parameter space of [WCE] CSPNe, the grid models have temperatures of $\approx$ 100,000, 125,000, 150,000, 165,000, and 200,000 K. The detailed emerging flux was calculated adopting a varying microturbulence velocity described by $\xi(r) = \xi_{min} + (\xi_{max} - \xi_{min})v(r)/v_\infty$, with ξ_{min} = 10 km s^{-1} near the photosphere and ξ_{max} = 50 km s^{-1}. The grid models were computed including many ionic species not considered in previous analyses and are described in Keller et al. (2011), Keller et al. (2012a,b).[1] Additional ad-hoc models were computed for each object with

[1] The grid covering the parameter regime of the [WC] CSPNe is available on-line at `http://dolomiti.pha.jhu.edu/`

Table 3. Ion superlevels and levels of the best-fitting final models for the central stars of NGC 6905, Sand 3, Pb 6, NGC 2867, and NGC 5189.

Element	I	II	III	IV	V	VI	VII	VIII	IX	X	XI
He	40,45	22,30	1								
C				49,64	1						
N					13,21	1					
O				29,48[a]	58,163	41,47	1				
Ne				45,355[a]	37,166	36,202	38,182	24,47	1		
Na						52,452	37,251	72,214	27,71	1	
Mg					43,311	46,444	54,476	1			
Si				22,33	33,71[a]	33,98[a]	1[a]				
P					16,62	1					
S						28,58	1				
Ar						30,205	33,174	57,72	1		
Ca						47,108[a]	55,514[a]	54,445[a]	35,367[a]	31,79[a]	1[a]
Fe						44,433[a]	41,252	53,324	52,490	43,210	1
Co							45,1000	50,1217	24,355	1	
Ni							37,308	113,1000	75,1217	1	

[a] These ionic species are not present in the best-fitting final models for the central stars of NGC 5189, Pb 6, and NGC 2867.

varying elemental abundances and microturbulence velocities, and including additional less abundant ions. The ions included in the final best-fitting models, together with the number of levels and superlevels adopted in the calculations, are given in Table 3.

3.2 Effects of the interstellar medium

In order to separate stellar features from interstellar absorptions due to neutral and molecular hydrogen along the line of sight, which greatly affect the far-UV spectra of these objects, we modelled them as described in Herald and Bianchi (2002, 2004a,b), assuming a temperature of the interstellar gas of 100 K, which is a typical value for the ISM, and determined the column densities. The derived interstellar parameters are given in Table 4, where $N(H\,\textsc{i})$ and $N(H_2)$ are the neutral and molecular hydrogen column densities, respectively. Fig. 4 shows the interstellar Ly α absorption seen in the observed spectra of Sand 3 and illustrates the fact that accounting for atomic hydrogen ISM absorption can affect the modelling of the N V $\lambda\lambda$ 1238.8, 1242.8 Å line. We did not attempt to model the ISM Ly α absorption in low resolution IUE spectra of CSPNe NGC 2867 and NGC 5189.

4 SPECTRAL ANALYSES

As the first step in the spectral analysis of the stellar lines, we estimated the terminal velocity of the wind from the short-wavelength edge of the strong P-Cygni profile of C IV λ 1548.2

`planetarynebulae.html`, where the user will find tables listing the available models and individual pages for every model, with information about the stellar parameters adopted, the ions considered and the synthetic spectra, as well as figures comparing the different models and identifying the spectral lines predicted.

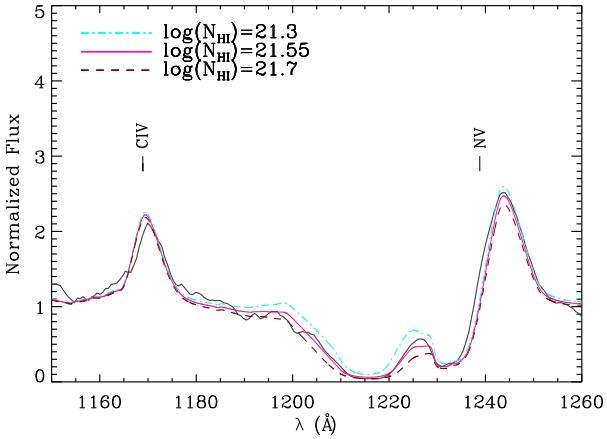

Figure 4. The interstellar Ly α absorption seen in the observed spectra of Sand 3 (continuous black line) is compared to our model, to which we applied the effect of different values of neutral hydrogen column density. The model shown has $T_* = 150$ kK, R_t =9.4 $R_\odot$ and $X_N = 0.07$

Table 4. Interstellar parameters adopted in the modelling.

Star	log $N(H\,\textsc{i})$[b]	log $N(H_2)$[c]	T_{gas} [K][d]	E_{B-V} [mag]	R_v
Pb 6	21.50	20.20	100	$0.25\pm^{0.05}_{0.05}$	3.1
NGC 5189	–	20.30	100	$0.23\pm^{0.07}_{0.03}$	3.1
NGC 2867	–	19.90	100	0.18[e]	3.1
NGC 6905[a]	21.00	19.50	100	$0.17\pm^{0.13}_{0.07}$	3.1
Sand 3	21.55	–	100	$0.40\pm^{0.05}_{0.05}$	3.1

[a] From Keller et al. (2011).
[b] From Ly α. $N(H\,\textsc{i})$ is given in units of cm^{-2}.
[c] From the absorption lines in the FUSE range. $N(H_2)$ is given in units of cm^{-2}.
[d] Assumed.
[e] Derived from the extinction quantity taken from Milingo et al. (2002b).

Å and also from the long wavelength component of the O VI $\lambda\lambda$ 1031.9, 1037.6 Å doublet whenever both or any of these lines were available, assuming a turbulence of 10 per cent the terminal velocity of the wind.

The spectra of [WCE] CSPNe are particularly poor in spectral lines of different ionization stages of the same element, and for this reason, the absence or presence of structures due to ions of different ionization potentials and the overall appearance of the spectra are also used to constrain temperature. As was shown by Keller et al. (2011), oxygen is one of the few elements producing strong lines of different ionization stages in the spectra of [WCE] CSPNe, with several O VI and two O V lines visible in the synthetic spectra throughout the temperature range of [WCE] CSPNe. As found by Keller et al. (2011), one important aspect about these O V lines, which can influence the determination of the stellar temperature, is their considerable increase in strength, in the synthetic spectra, when less abundant ions are included into the calculation, especially Mg, Na, Co, and Ni. These ions are not included

in the grid models, because of computational limitations, but we include them in our final best-fitting models, as we show below.

The most important line diagnostics we rely upon when constraining the surface temperatures of these stars are the Ne VII λ 973.3 Å and O VI $\lambda\lambda$ 1031.9, 1037.6 Å P-Cygni profiles and the O V λ 1371.3 Å and $\lambda\lambda$ 2781.0, 2787.0 Å lines. The Ne VII λ 973.3 Å line is a useful temperature diagnostic, because its synthetic profile is substantially weakened by the decrease in temperature in the [WCE] parameter regime and because it shows little sensitivity to mass loss at model temperatures of 100,000 and 125,000 K, in the parameter regime covered by our model grid (Fig. 1). At these temperatures, it also shows little sensitivity to neon abundance, as shown by Keller et al. (2011). A similar behaviour with temperature is observed in the synthetic O VI $\lambda\lambda$ 1031.9, 1037.6 Å doublet, whose strength also increases towards models with T_* =165,000 K and which is not particularly sensitive to variations in mass loss at model temperatures of 100,000 and 125,000 K. Thus, the strong Ne VII λ 973.3 Å and O VI $\lambda\lambda$ 1031.9, 1037.6 Å P-Cygni profiles observed in all the objects with FUSE spectra shown here, immediately point towards models of T_* =150,000 K or 165,000 K, with the latter allowing for even stronger line profiles, concomitantly with good fits to the remaining lines.

One of the most striking differences among the observed spectra of the studied stars, which are otherwise very similar, is the strength of the O V lines. The central star of NGC 6905 and Sand 3 show much stronger lines than is seen in the spectra of NGC 5189 and of Pb 6, or even than is present on the nebula-dominated IUE spectra of NGC 2867. This characteristic, along with the line appearance, can further constrain temperature: the appearance of the O V λ 1371.3 Å line profile also excludes models with T_* =100,000 and 125,000 K, since none of the observed line profiles show the deep P-Cygni absorption components that are seen in these models. Also, although the grid models with T_* =150,000 K and 165,000 K show weak O V lines for mass-loss rates that allow reasonable fits of the overall observed spectra, their synthetic profiles do become much stronger through the addition of further ions into the calculations, with the T_* =150,000 K models producing O V profiles considerably stronger than models with T_* =165,000 K. We thus concluded that the central star of NGC 6905 and Sand 3 are cooler than the other three objects and best fit by models of T_* =150,000 K, while the central stars of NGC 2867, NGC 5189, and Pb 6 best-fitting models have T_* =165,000 K.

Hotter models, with T_* =200,000 K, were also computed by us. However, they do not

fit well the observed spectra: at the same time, the models show too weak O VI $\lambda\lambda$ 1031.9, 1037.6 Å lines and too strong He II λ 1640.4 Å and C IV $\lambda\lambda$ 1107.6, 1107.9 Å, $\lambda\lambda$ 1168.8, 1169.0 Å and $\lambda\lambda$ 1548.2, 1550.8 Å lines, such that the discrepancy is too big to be solved by different abundance patterns. The 200,000 K models also predict Ne VII λ 973.3 Å lines with shallower and narrower absorption components than what is seen in the observations and no O V emission lines.

Another factor that influences the appearance of the spectral lines in these stars is how dense their wind is. Schmutz et al. (1989) have introduced the so called transformed radius, defined as $R_{\rm t} = R_*[(v_\infty/2500 \text{ km s}^{-1})/(\dot{M}/10^{-4} \text{ M}_\odot\text{yr}^{-1})]^{2/3}$. Models of the same transformed radius that also have identical temperature, composition, and terminal velocity - that is, models where $R_*/\dot{M}^{2/3}$ is the same - are known to have similar ionization structure and temperature stratification and to lead to very similar wind line spectra (Hamann et al. 1993). In this work, we will constrain the transformed radius rather than the mass-loss rate, because deriving mass-loss from R_t depends on a measurement of the stellar radius, which depends on the distance and distances to Galactic CSPNe are commonly not well known. On top of this, the absence of strong absorption lines not contaminated by wind emissions in the spectra of [WCE] stars prevents us from measuring $\log g$.

The overall strength of all available wind lines was used by us to constrain the transformed radius. Among them, the He II λ 1640.4 Å - whenever not strongly affected by nebular emission - is especially useful due to its little sensitivity to temperature in the parameter regime covered by the model grid for [WCE] stars. The behaviour of the synthetic spectral lines apparent in the spectra of [WCE] stars with stellar parameters was extensively described in Keller et al. (2011).

After having used the grid of synthetic spectra to constrain stellar temperature and transformed radius, we then extended the analysis by exploring various abundances for the main elements and different microturbulence velocities, as well as by including additional elements into the calculations. The temperature steps of our model grid, in the [WCE] regime, are small enough that subsequent models do not show strong variations of line diagnostics. That is the reason for the non-homogeneous temperature intervals in our model grid. In our ad-hoc analysis, temperature was therefore not varied further. At each likely temperature, a number of models was calculated with different elemental abundances, as to ensure that different abundance patterns would not affect the constraining of temperature.

For all objects studied here, we found that a microturbulence velocity higher than that

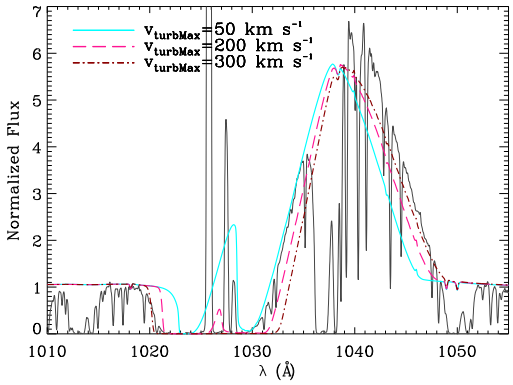

Figure 5. CSPN NGC 5189 observed O VI $\lambda\lambda$ 1031.9, 1037.6 Å line (black continuous line) is compared with a grid model with $T_* = 165$ kK, $R_t = 9.9 R_\odot$, $v_\infty = 2500$ km s^{-1} recomputed to account for different microturbulence velocities.

adopted in the grid models (Table 5) improves the fits to the O VI $\lambda\lambda$ 1031.9, 1037.6 Å P-Cygni profile, as shown in Fig. 5, and also to the C IV $\lambda\lambda$ 1548.2, 1550.8 Å line.

4.1 Results for individual objects

The observed spectra and final best-fitting models for the individual objects are shown in Figs. 6, 7, and 8. The parameters of our best-fitting models are given in Table 5. The uncertainties in stellar temperature are given in the sections on the individual objects. Whenever far-UV, UV, and near-UV spectra are available for an object, we estimate the uncertainty in T_* to be roughly half the interval between the values adopted in our grid of synthetic spectra. When, as is the case of NGC 2867 and Sand 3, not all the necessary line diagnostics are available, the uncertainties in temperature are deemed larger. The uncertainties in the mass-loss rate are dominated by the uncertainties in the distance and in the clumping filling factor, which was assumed a fixed parameter throughout this work. We can typically constrain R_t within $\pm$ 2.0 R$_\odot$. Assuming the stellar parameters of the best-fitting models of the various sample objects, we estimate the uncertainties of the carbon and helium mass fraction are about $\pm$0.10, as illustrated in Fig. 9, and the uncertainties of the oxygen and nitrogen mass fractions to be about $\pm$0.06 (Fig. 17 from Keller et al. (2011) illustrates the impact of different oxygen abundances on the synthetic spectra) and $\pm$0.01 (Fig. 10), respectively. We have used the far-UV Ne VII and Ne VI features in the FUSE spectra to determine the neon mass fractions. However, as we discuss further below, Ne features appear in the synthetic spectra at longer wavelengths, which are not observed, perhaps due to uncertainties in the atomic data. The Ne VII λ 973.3 Å line, however, has been used to infer enhanced neon

abundances in PG 1159 stars by Herald et al. (2005) and Werner et al. (2004). The atomic data used for the λ 973.3 Å Ne VII line are described in Herald et al. (2005).

The observed spectra shown in Figs. 7 and 8 were obtained with different instruments and thus, differ in spectral resolution. Sand 3, NGC 6905, and Pb 6 STIS spectra were obtained with different apertures and thus display different line spread functions (LSFs) as well. The synthetic spectra were convolved with the corresponding LSFs when being compared to STIS observations and with Gaussians of appropriate FWHM when compared to IUE and FUSE data.

4.1.1 CSPN NGC 6905 and Sand 3

CSPN NGC 6905 and Sand 3 are the two stars for which we inferred lower temperatures: $T_* = 150\pm^{8}_{13}$ kK for NGC 6905 and $T_* = 150\pm^{8}_{25}$ kK for Sand 3, the difference in error bars being due to the lack of FUSE spectra available for Sand 3, which deprives the analysis of the far-UV O VI and Ne VII P-Cygni profiles, which are the line diagnostics that most clearly separate models of 125,000 and 150,000 K. We determined terminal velocities of the wind of v_∞ =2000±200 and 2200±200 km s^{-1} respectively. Their STIS spectra are very similar and both stars show O V lines much stronger than in all other sample objects. Two of the most conspicuous differences between the spectra of these two stars are the strong N V $\lambda\lambda$ 1238.8, 1242.8 Å P-Cygni profile seen in Sand 3's spectrum and absent from NGC 6905's and the even stronger O V $\lambda\lambda$ 2781.0, 2787.0 Å line observed in Sand 3. From the absence of a N V $\lambda\lambda$ 1238.8, 1242.8 Å line profile in the observed spectra of NGC 6905, we derived, in Keller et al. (2011), an upper limit to its N mass fraction of 5.5×10^{-4}, while for Sand 3, a much higher abundance of $X_N = 0.07$ was found. For both stars we found the same oxygen mass fraction, $X_O = 0.08 \pm 0.06$. Although neither best-fitting model for either star reproduces the observed intensity of the O V $\lambda\lambda$ 2781.0, 2787.0 Å line, our best-fitting model for Sand 3 predicts a stronger line than our model for CSPN NGC 6905, which is due to the lower value of transformed radius adopted in the former model ($R_t = 9.4 \pm 2.0$ R$_\odot$ for Sand 3 and $R_t = 10.7 \pm 2.0$ R$_\odot$ for NGC 6905). Because no FUSE spectra are available for Sand 3, we simply kept the Ne abundance used in the grid models.

Carbon and helium mass fractions derived by us for CSPN NGC 6905 ($X_C = 0.45 \pm 0.10$, $X_{He} = 0.45 \pm 0.10$) and Sand 3 ($X_C = 0.55 \pm 0.10$, $X_{He} = 0.28 \pm 0.10$) are quite different, which illustrates the fact that the overall appearance of [WCE] spectra is mainly governed

by temperature and mass loss, and He and C abundances play only a secondary role, with big changes in abundance producing minor changes in line strength.

Optical and low resolution IUE spectra of Sand 3 were previously analysed by Koesterke and Hamann (1997b), using non-LTE, homogeneous, spherically symmetric expanding atmosphere models, which included helium, carbon, oxygen and nitrogen in the calculations. They found $v_\infty = 2200$ km/s, $T_* = 140000$ K, and $R_t = 3.0$ R$_\odot$. As for the elemental mass fractions, they derived $X_{He} = 0.615$, $X_C = 0.26$, $X_O = 0.12$ and $X_N = 0.005$. Values of v_∞, T_*, and X_O are in agreement with those derived in this work within the error bars. X_{He}, X_C, and X_N are in strong disagreement. In a previous work, Barlow and Hummer (1982) derived He, C, and O mass fractions that are close to the values derived by us. A previous analysis of CSPNe NGC 6905 was discussed in Keller et al. (2011).

4.1.2 CSPN NGC 2867

The O VI $\lambda\lambda$ 1031.9, 1037.6 Å P-Cygni profile of CSPN NGC 2867 is clearly narrower than those observed in NGC 5189 and Pb 6 spectra and thus we derived v_∞ =2000±250 km s^{-1} for the central star of NGC 2867. If indeed the nebula-dominated low resolution IUE spectra of NGC 2867 contains the stellar flux, we can set an upper limit to the strength of the O V lines and thus better constrain the temperature. Since no strong O V lines are seen, models with stellar temperatures of 165,000 K would be favoured. If not, we can only leverage on FUSE spectra to discern between model temperatures. However, this spectral region does not show remarkable differences between models of 150,000 and 165,000 K, although it rules out models of $T_* \leqslant 125{,}000$ K which do not produce the strong Ne VII and O VI P-Cygni profiles observed. Models of 165,000 K do produce, however, somewhat stronger Ne VII and O VI lines, while concomitantly producing reasonable fits for the other available lines, than models of 150,000 K, in which these lines appear somewhat weaker than observed. We thus derived $T_* = 165\pm^{18}_{20}$ kK for the central star of NGC 2867, $R_t = 8.5 \pm 2.0$ R$_\odot$, $X_C = 0.25 \pm 0.10$, $X_{He} = 0.60 \pm 0.10$ (even though we did not attempt a fit of the He II 1640.4 Å line due to the heavy nebular contamination in the observed spectra of this star, its helium mass fraction can be determined for it is the complement of the sum of all other elemental mass fractions considered in the calculations), and $X_O = 0.10 \pm 0.06$. Since no nitrogen line is available in the FUSE range, we merely kept the nitrogen mass fraction adopted in our grid models.

Koesterke and Hamann (1997a) analysed optical and IUE spectra of a series of CSPNe, among them the central stars of NGC 2867, NGC 5189, and Pb 6 using a non-LTE radiative transfer code that considers homogeneous winds and He, C, O, and N opacities. They found, for NGC 2867, $v_\infty = 1800$ km s^{-1}, $T_* = 141000$ K, and $R_t = 4.0$ R$_\odot$. The elemental mass fractions derived by them are $X_{He} = 0.66$, $X_C = 0.25$, and $X_O = 0.09$. Their derived values of v_∞, X_{He}, X_C, and X_O are in agreement within the errors.

4.1.3 CSPN Pb 6

CSPN Pb 6, as well as NGC 5189's central star, displays wider O VI $\lambda\lambda$ 1031.9, 1037.6 Å and C IV $\lambda\lambda$ 1548.2, 1550.8 Å P-Cygni profiles than the other sample objects. We determined a terminal velocity of the wind of v_∞ =2500±200 km s^{-1} for this star. The strong O VI $\lambda\lambda$ 1031.9, 1037.6 Å far-UV P-Cygni profile and weak O V lines observed in CSPN Pb 6 suggest a temperature of $T_* = 165\pm^{18}_{8}$ kK. The derived transformed radius and elemental abundances are: $R_t = 9.9 \pm 2.0$ R$_\odot$, $X_C = 0.35 \pm 0.10$, $X_{He} = 0.49 \pm 0.10$, $X_O = 0.12 \pm 0.06$, $X_N = 0.03 \pm 0.01$.

Koesterke and Hamann (1997a) found for this star: $v_\infty = 3000$ km s^{-1}, $T_* = 140000$ K, $R_t = 4.5$ R$_\odot$, $X_{He} = 0.617$, $X_C = 0.24$, $X_O = 0.14$, and $X_N = 0.003$. Only X_O is in agreement with values derived in this work within the errors. The stellar temperature derived by us is considerably higher and the terminal velocity is much lower. Especially discrepant is the nitrogen mass fraction, whose value derived by us is 10 times that of the previous analysis.

4.1.4 CSPN NGC 5189

As in the case of CSPN Pb 6, we found a terminal velocity of the wind of v_∞ =2500±250 km s^{-1} for the central star of NGC 5189. The presence of very strong far-UV Ne VII and O VI P-Cygni profiles in its FUSE spectrum, accompanied by weak O V lines, led us to derive a stellar temperature of $T_* = 165\pm^{18}_{8}$ kK, similarly to Pb 6 and NGC 2867. We derived, for the central star of NGC 5189, $R_t = 9.9 \pm 2.0$ R$_\odot$ (same as for Pb 6), $X_C = 0.25 \pm 0.10$ (same as for NGC 2867), $X_{He} = 0.58 \pm 0.10$, $X_O = 0.12 \pm 0.06$ (same as for Pb 6), $X_N = 0.01 \pm 0.01$.

Although we regard the He II λ 1640.4 Å line as a mere upper limit to the stellar contri-

Table 5. Parameters of our best-fitting models for the sample objects and distance dependent parameters. X_{He}, X_C, X_N, X_O, and X_{Ne} are the helium, carbon, nitrogen, oxygen, and neon mass fractions, respectively. For the discussion on the derived parameters and errors, see text. Results by other authors are also shown.

Object	Pb 6		NGC 6905			NGC 5189		Sand 3			NGC 2867	
	t.w.	KH1997a	t.w.	M2007	KH1997a	t.w.	KH1997a	t.w.	KH1997b	BH1982	t.w.	KH1997a
T_* [kK]	165	140	150	149.6	141	165	135	150	140	200	165	141
R_t [$R_\odot$]	9.9	4.5	10.7	10.5	3.4	9.9	5.0	9.4	3.0		8.5	4.0
v_∞ [km/s]	2500	3000	2000	1890	1800	2500	3000	2200	2200	2700	2000	1800
X_{He}	0.49	0.617	0.45	0.49	0.60	0.58	0.757	0.28	0.615	0.38	0.60	0.66
X_C	0.35	0.24	0.45	0.40	0.25	0.25	0.16	0.55	0.26	0.54	0.25	0.25
X_O	0.12	0.14	0.08	0.10	0.15	0.12	0.08	0.08	0.12	0.08	0.10	0.09
X_N	0.03	0.003	0.00011	<0.001	0	0.01	0.003	0.07	0.005		0.01[b]	0
X_{Ne}	0.01		0.02			0.04		0.02[b]			0.04	
ξ_{max} [km/s]	200		150			200		150			200	
d[c][kpc]	4.38		1.70			0.55		0.80[a]			1.84	
distance dependent parameters												
R_* [$R_\odot$]	0.06		0.09			0.03		0.12[a]			0.05	
$\log L/L_\odot$	3.43		3.56			2.73		3.84[a]			3.15	
$log\dot{M}$ [$M_\odot yr^{-1}$]	-7.29		-7.21			-7.81		-6.89[a]			-7.50	

t.w.=this work; KH1997a=Koesterke and Hamann (1997a); KH1997b=Koesterke and Hamann (1997b); M2007=Marcolino et al. (2007b), BH1982=Barlow and Hummer (1982)

[a] Values obtained assuming $\log L/L_\odot$=3.84.

[b] Not constrained. Value assumed on the grid models was kept.

[c] Distances from Table 1.

bution, due to the evidence of nebular contamination presented above, and despite the fact that we derived the parameters of our best-fitting model without attempting to precisely match the observed intensity of this line, it is, however, reproduced in the final model. In order to maintain the overall fit to the other wind lines and at the same time decrease the strength of the He II 1640.4 Å line, the helium mass fraction would have to be severely lowered, at the same time that the value of mass-loss rate would have to be decreased as to allow the correspondent increase in carbon and oxygen mass fraction that need to occur to assimilate the decrease in the helium mass fraction. Mass fractions of neon and nitrogen would also have to be revised up to compensate for the lower mass-loss rate. We computed models to explore this alternative. They result in considerably worse fits to the O VI $\lambda\lambda$ 1031.9, 1037.6 Å doublet, which is now very weak in comparison to the observations. This incongruence illustrates the need for higher resolution UV spectra of CSPNe.

The stellar parameters derived by Koesterke and Hamann (1997a) for NGC 5189 are v_∞ = 3000 km/s, T_* = 135000 K, R_t = 5.0 $R_\odot$, and X_{He} = 0.757, X_C = 0.16, X_O = 0.08, and X_N = 0.003, in mass fractions. Only carbon and oxygen mass fractions derived by them agree within the errors with those found by us. As in the case of Pb 6, a much higher stellar temperature and considerably lower terminal velocity of the wind and helium mass fraction were derived by us, besides a 10 times higher nitrogen mass fraction.

4.2 The problematic near-UV region

In the studied objects, the spectral region between 1700 and 3200 Å is problematic. The available spectra have worse resolution in this region, which is full of structures that make the determination of the stellar continuum uncertain. In the region between 1700 and 2400 Å, observed features both in absorption and in emission are not reproduced by our best-fitting models or grid models of any temperature and mass-loss rate. The region between 2150 and 2300 Å is particularly challenging. There is, in this region, a strong feature observed in the central stars of NGC 6905, NGC 5189, Pb 6, and Sand 3, showing an emission component on the red side and an absorption one on the blue side. This feature reminds us of a P-Cygni profile in the observed spectra of Pb 6 and of NGC 6905 central stars, but in the noisier and low resolution spectra available for NGC 5189 and Sand 3, the blue side resembles a simple absorption. Our models are able to reproduce the red side of these features, in the case of NGC 6905 and of NGC 5189, but not the blue absorptions that are located very close to the broad feature of the interstellar extinction curve at 2175 Å, which is related to graphite grains (Draine and Malhotra 1993). Another difficulty in modelling these stars consists of weak Ne V and Ne VI lines that are predicted throughout the near-UV by the models, but are not observed. While we checked CMFGEN's neon atomic data files for consistency with the Atomic Line List (`http://www.pa.uky.edu/~peter/atomic/`) and found no discrepancy, there may be uncertainties in the atomic data. The neon atomic data are primarily taken from the Opacity Project (Seaton 1987; Seaton et al. 1994) and the Atomic Spectra Database at the NIST Physical Measurement Laboratory.

4.3 Argon and Iron

In Keller et al. (2011), we found that a model with 10 times the argon solar abundance produces an Ar VII λ 1063.55 Å line which approximately reproduces the observed line profile in that spectral region of CSPN NGC 6905. In Fig. 6, the best-fitting models for NGC 5189 and NGC 2867 also have the same argon overabundance. However, the shapes of the observed and synthetic profiles disagree, challenging the identification of this line.

In all best-fitting models, we assumed a strong iron underabundance of one hundredth of the solar value, since higher values would entail the appearance of a number of non-observed Fe X lines in the synthetic spectra (Keller et al. 2011). These lines are not, however, observed

in PG1159 stars for which solar iron abundances were found by Werner et al. (2010, 2011) and there may be strong uncertainties in their computed wavelengths.

4.4 Reddening

Having constrained the main stellar parameters through the analysis of the strength of spectral lines, we now compare the slope of the observed spectral continuum of each sample object to that of our best-fitting models reddened by different values of colour excess as shown in Fig. 11. We adopted Cardelli et al. (1989) extinction curves with $R_V = 3.1$. The results are listed in Table 4. In the case of NGC 2867, which is shown separately in Fig. 12, we had to take into consideration the contribution from the nebular continuum, which heavily affects wavelengths longer than Ly α. We estimated the nebular continuum emission using the code described in Bianchi et al. (1997), which accounts for two-photon, H and He recombination, and free-free emission processes. Nebular parameters were taken from the literature (Milingo et al. 2002a,b) and they include the electron density, electron temperature, observed Hβ flux, helium-to-hydrogen ratio, ratio of doubly to singly ionized helium and the extinction quantity (c). We found $E(B-V) = 0.18$, which corresponds to the value of c found in the literature, to allow for an overall good match between observed continuum of NGC 2867 and the sum of model stellar and nebular emissions.

4.5 Discussion

Fig. 13 shows the evolutionary tracks of Miller Bertolami and Althaus (2006) in the $\log(T_{eff}) \times \log(L)$ diagram and the position of our sample objects. Luminosities are based on distances taken from the literature and are shown in Table 5. Sand 3 was omitted from the figure, because we were unable to find measurements of its distance in the literature. The sample objects intercept the evolutionary tracks at 0.565 and 0.584 solar masses. The distance values adopted from the literature place the central stars of NGC 6905 and Pb 6 on the verge of entering the WD cooling track, while they put the central stars of NGC 5189 and NGC 2867 already within it, in a region where PG1159 stars are expected. [WCE]-type CSPNe are, however, expected to populate the region of constant luminosity of the evolutionary tracks in the HRD, which, at the temperatures derived here, would require higher luminosities and thus, greater distances.

Among the five objects analysed in this work, Sand 3 is the only one whose derived

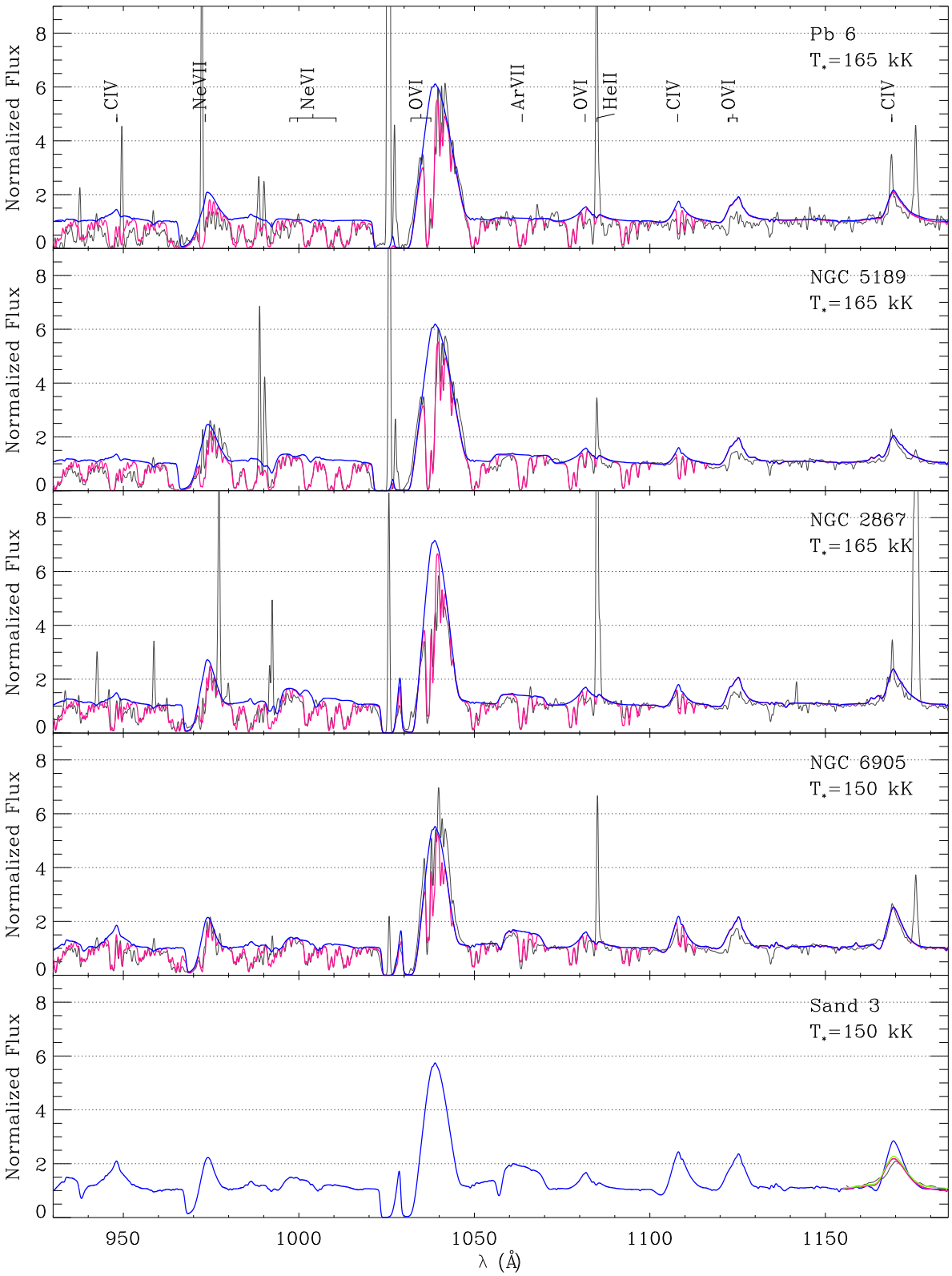

Figure 6. FUSE spectra (black line) of CSPNe Pb 6, NGC 5189, NGC 2867, and NGC 6905 shown together with our best-fitting models, with (pink) and without (blue) the effects of interstellar absorption due to molecular and atomic hydrogen. The observed and synthetic spectra were degraded to a 0.5 Å resolution for clarity. No FUSE is spectrum is available for Sand 3. We, however, still show the synthetic spectra prediction for this wavelength interval with a 0.5 Å resolution for comparison with results for the other sample objects. HST/STIS spectra of this star comprehend the C IV $\lambda\lambda$ 1168.8, 1169.0 Å line, which is shown here in black. In pink and green we show our best-fitting model for Sand 3, with and without Ly α absorption, convolved with the appropriate HST/STIS LSF. The identifications of stellar lines shown in this and following figures correspond to the strongest lines predicted by the models at each spectral region.

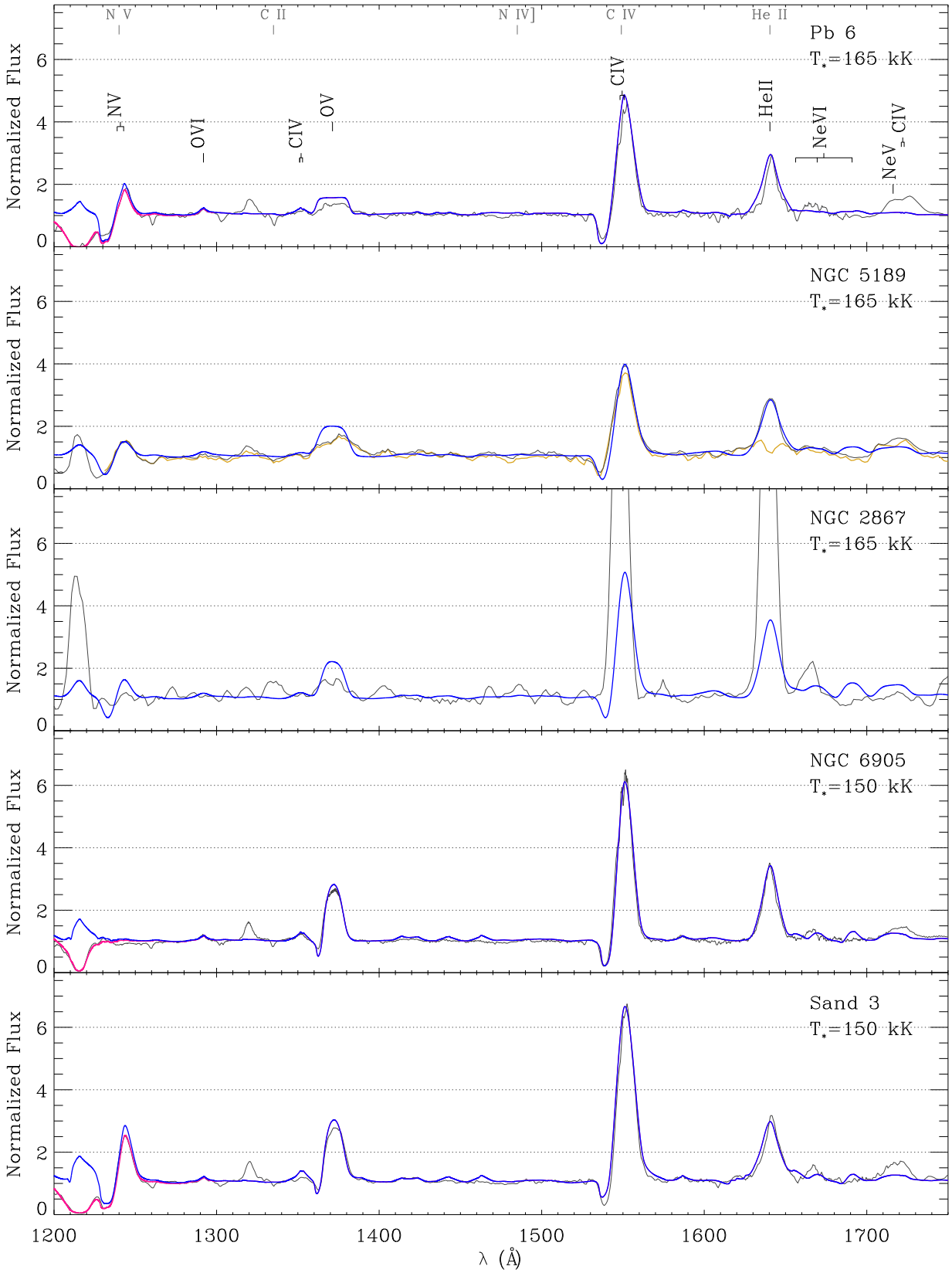

Figure 7. Observed spectra of the sample objects (black) in the region between 1200 and 1750 Å shown with our best-fitting models, with (pink) and without (blue) ISM absorption, degraded to match the resolution of the observations (see table 2). For CSPN NGC 5189 we also show the subtracted spectrum from Fig. 3, in yellow. The grey labels on the top part of the figure identify the position of commonly present nebular lines.

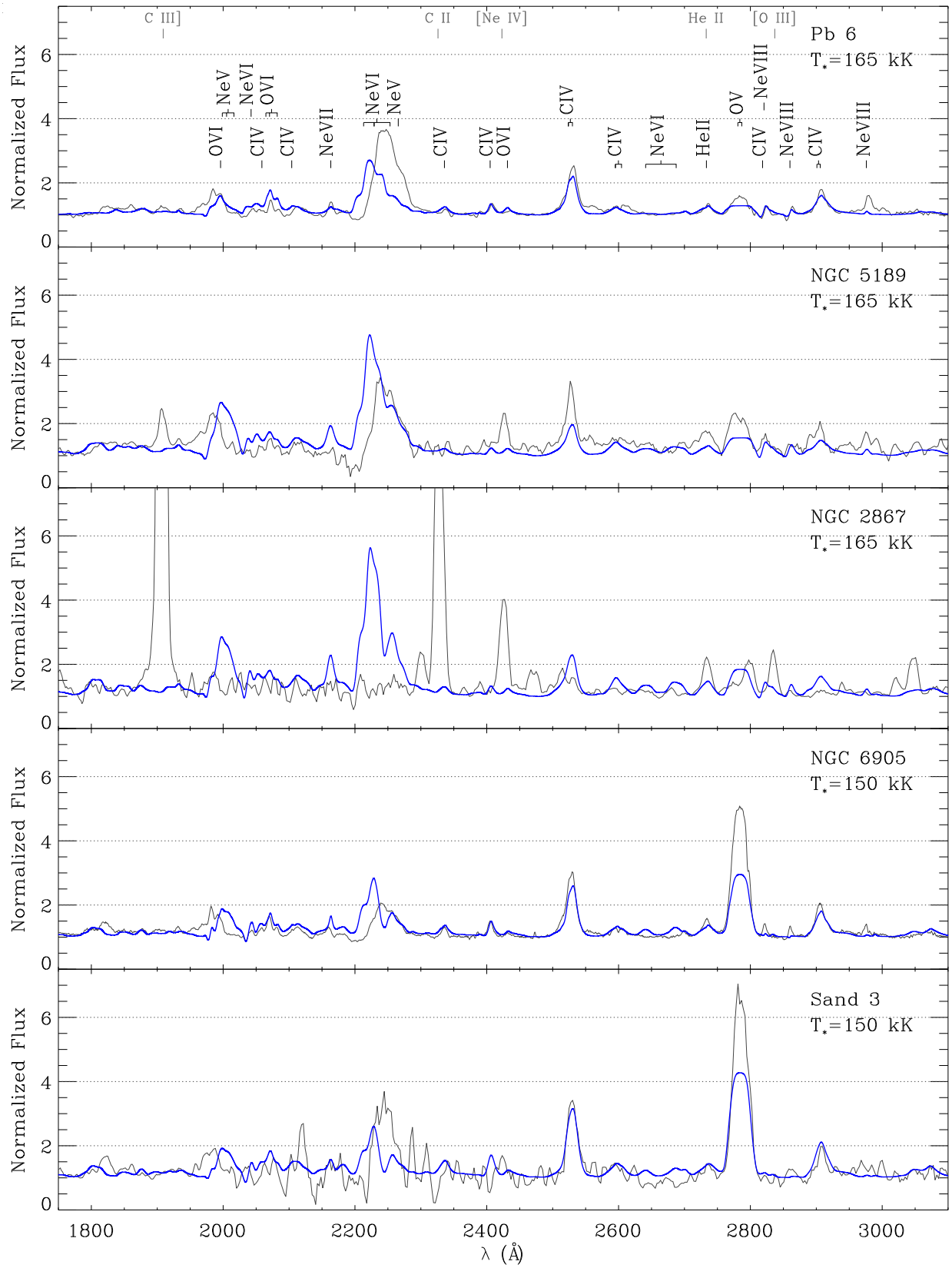

Figure 8. Near-UV observed spectra (black) together with our best-fitting models to the sample objects (blue).

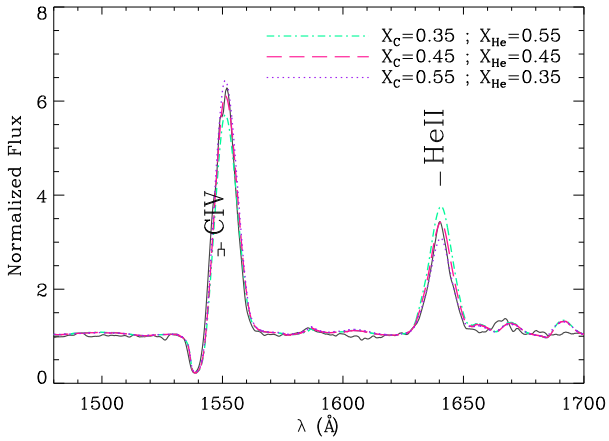

Figure 9. Observed spectrum of the central star of NGC 6905 (black continuous line) and models with $T_* = 150$ kK, $R_t = 10.7 R_\odot$, $v_\infty = 2000$ km s^{-1} and different carbon and helium abundances.

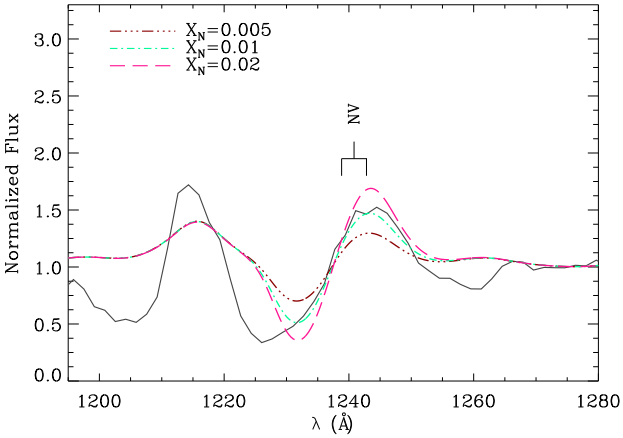

Figure 10. Observed spectra of the central star of NGC 5189 (black continuous line) and models with $T_* = 165$ kK, $R_t = 9.9 R_\odot$, $v_\infty = 2500$ km s^{-1} and different nitrogen abundances.

abundances seem to place it outside the range of values found in the literature for [WC] stars, since it shows, according to Table 5, a quite low helium abundance of 0.28 in mass fraction (not significantly lower, however, than the lowest value of helium mass fraction found for PG1159 objects, which is 0.30). The derived He, C, and O abundances, in mass fractions, of our sample objects are in the intervals: $X_{He} = 0.28 - 0.60$, $X_C = 0.25 - 0.55$, and $X_O = 0.08 - 0.12$ (see Fig. 14). It is generally believed that [WCL]-type CSPNe evolve into [WCE] objects and thus, both classes are expected to present somewhat similar carbon to helium ratios. However, previous analyses have shown the carbon content in [WCE]-type stars to be lower than what is seen in [WCL] objects, with $0.19 < C : He < 0.7$ for [WCE] stars (Koesterke and Hamann 1997a,b) and $C : He$ typically higher than 1 for [WCL] stars (Leuenhagen et al. 1996). The wide range of values found by us in this work seems to argue against this notion: we found $C : He$ =0.42, 0.43, 1.0, 0.71, 1.96 for the central stars of

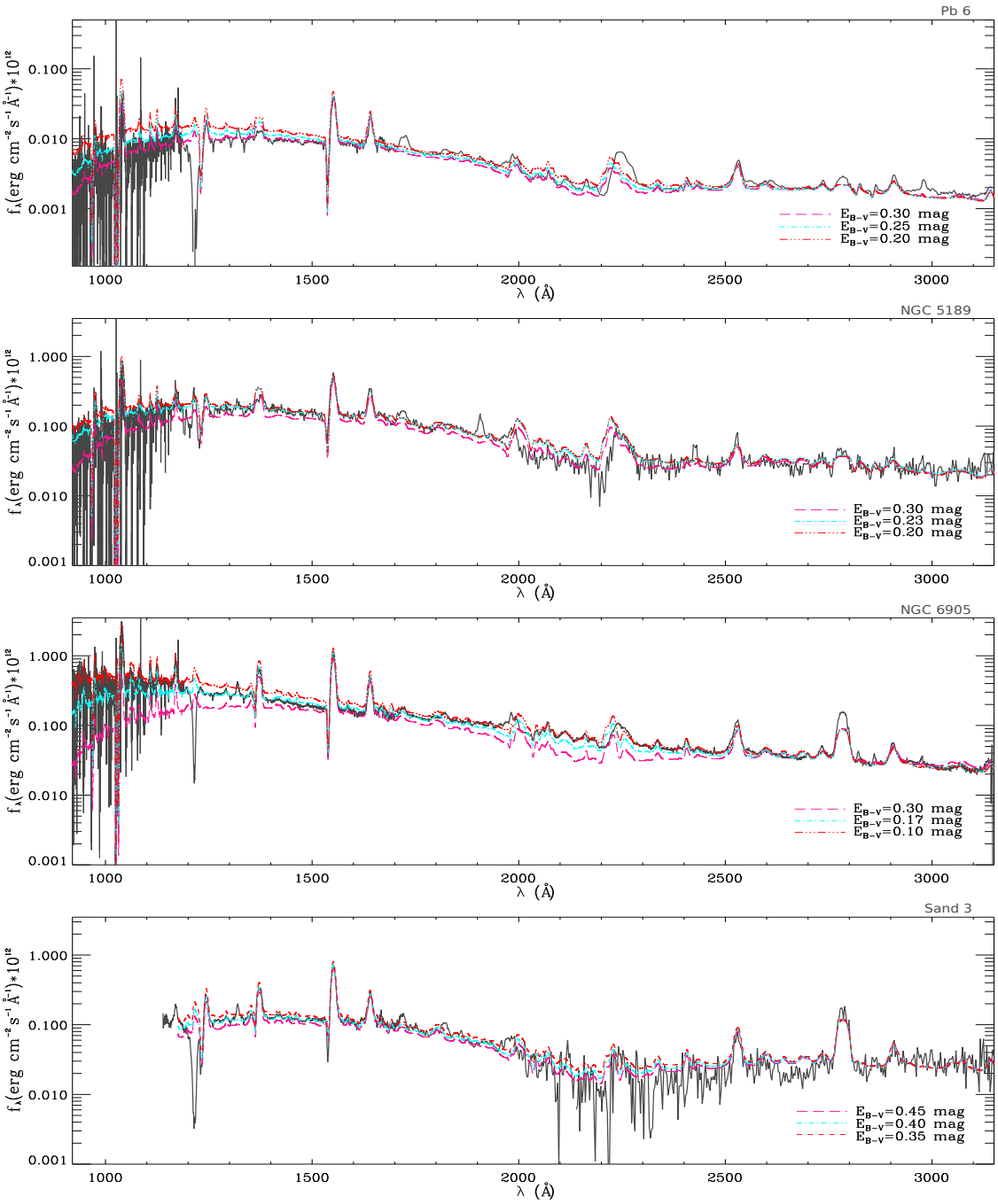

Figure 11. The observed spectra of the sample objects (continuous black lines), except for NGC 2867, are shown together with our best-fitting models reddened by different values of the colour excess. We used the Cardelli et al. (1989) extinction curves, with $R_V = 3.1$.

NGC 2867, NGC 5189, NGC 6905, Pb 6, and Sand 3, respectively. This is in line with the results from Crowther et al. (2003) and Marcolino et al. (2007b) that found no systematic discrepancies in the $C : He$ ratios between [WCL] and [WCE] stars.

Values of the nitrogen mass fraction derived in the literature range from $< 3 \times 10^{-5}$ (see Werner and Herwig 2006, and references therein) to 0.04 (Leuenhagen et al. 1993). We have

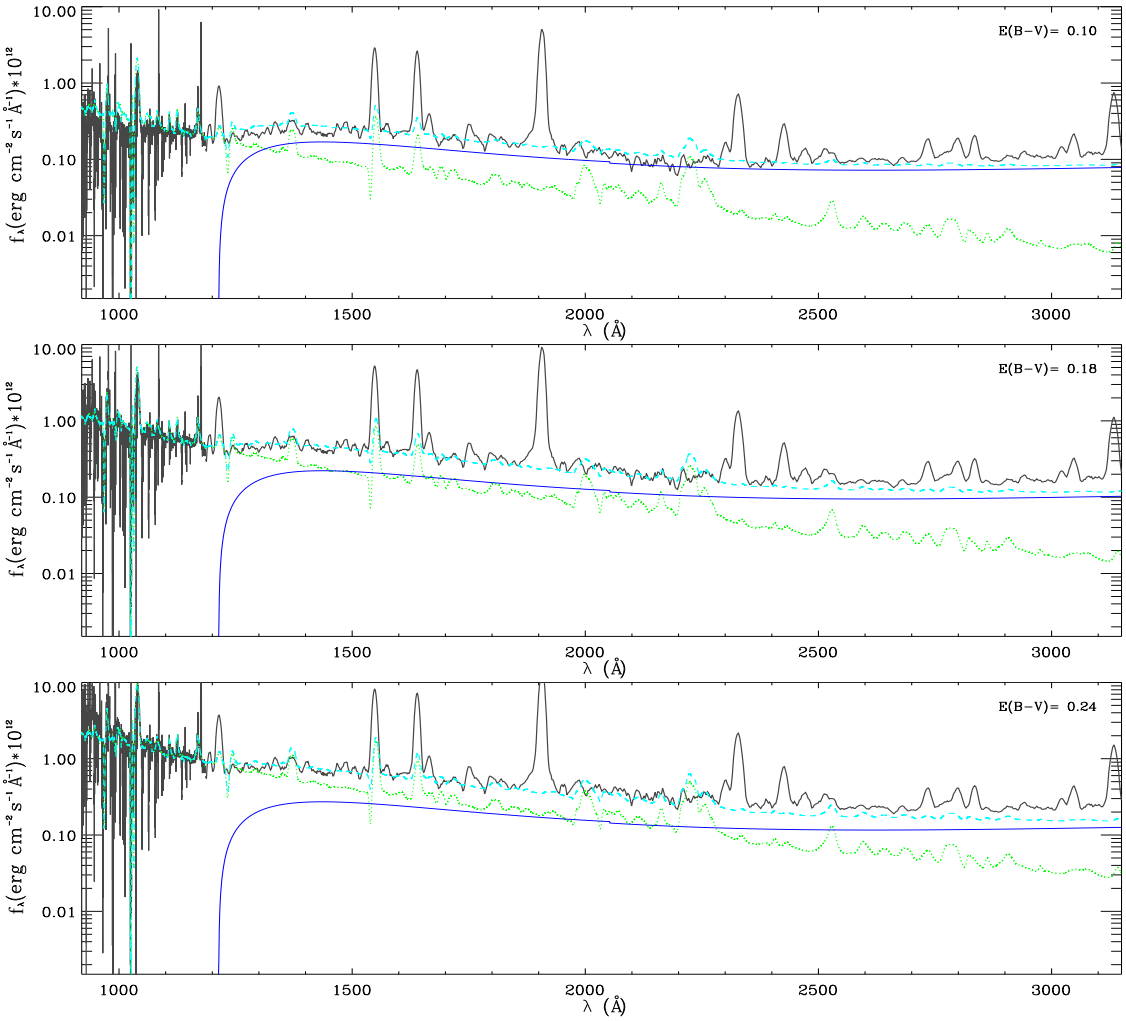

Figure 12. The observed spectra of NGC 2867 (continuous black lines) dereddened adopting different values of the colour excess is shown together with our best-fitting model for the stellar spectrum (green dotted line), a model for the nebular continuum (blue continuous line) and the sum of both models (cyan dashed line). We used the Cardelli et al. (1989) extinction curves, with $R_V = 3.1$.

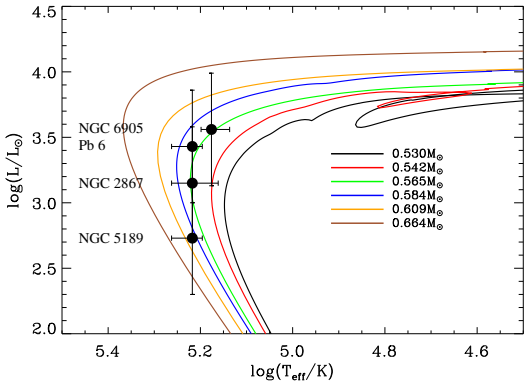

Figure 13. HR diagram with evolutionary tracks from Miller Bertolami and Althaus (2006). The open circles correspond to the sample objects. Sand 3 was omitted from it, because, to the best of our knowledge, there is no measurement of its distance in the literature.

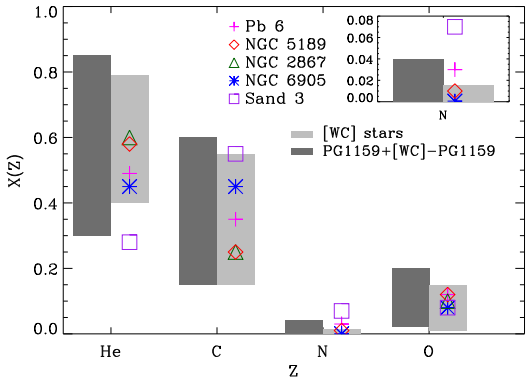

Figure 14. The abundance intervals of PG1159, [WC]-PG1159 and [WC] stars (as found from the literature) are compared to the values determined in this work.

derived an upper limit of 5.5×10^{-4} for the nitrogen abundance of NGC 6905, which would indicate it is the product of a LTP or even an AFTP. The central stars of NGC 5189, Pb 6 and Sand 3, on the other hand, all show conspicuous N V $\lambda\lambda$ 1238.8, 1242.8 Å lines that led to derived nitrogen mass fractions of 1, 3, and 7 per cent, respectively, pointing to the occurrence of VLTP events.

We have not included hydrogen in our grid models or in the best-fitting models presented in this work. However, we calculated exploratory models which indicate an upper limit to the hydrogen mass fraction of 20 per cent for our sample objects.

Neon abundances of about 2 per cent have been reported for a number of PG1159 stars (Werner et al. 2004), which is in agreement with stellar evolution models that predict a neon mass fraction of about 2 per cent in the intershell region. In this work, modelling of the far-UV Ne VII and Ne VI features led us to infer neon mass fractions between 1 and 4 per cent.

5 CONCLUSIONS

We have analysed UV spectra from 5 of the hottest known [WCE]-type CSPNe, which are the central stars of NGC 2867, NGC 5189, NGC 6905, Pb 6, and Sand 3. The analysis was performed using our extensive grid of synthetic spectra, calculated with CMFGEN, which allowed us to constrain temperatures, transformed radii, and terminal velocities of the wind, in a uniform and systematic way. The analysis was then refined by exploring other parameters, such as elemental abundances and microturbulence velocities, besides adding further elements and ionic species into the calculations.

We applied the effects of interstellar absorption due to neutral and molecular hydrogen to our best-fitting models and determined their column densities and after the stellar parameters were constrained based on line diagnostics, we compared the observed slope of the stellar continua to our best-fitting models reddened using different values of colour excess.

We derived $T_* = 150000$ K for CSPNe NGC 6905 and Sand 3 and $T_* = 165000$ K for the central stars of NGC 2867, NGC 5189, and Pb 6. This result corresponds to an upward revision of the temperatures derived for the latter three objects, in comparison with previous analyses (for Sand 3 and the central star of NGC 6905, the derived temperatures agree with previous results within the errors), a fact that has two reasons: the first one is the inclusion of several less abundant ions into the calculations, as described above, that caused the O V lines to increase in intensity without altering other line diagnostics, allowing us to fit the observed spectra with hotter models. The O V lines are important temperature diagnostics and allowed us to separate between models of 150 and 165 kK; The second reason is the modelling of the O VI $\lambda\lambda$ 1031.9, 1037.6 Å and Ne VII λ 973 Å lines in the FUSE range, which had not been modelled in previous analyses of these three stars and which are stronger in our grid models of 165 kK. The terminal wind velocities of the sample objects were found to range from 2000 to 2500 km s^{-1}. Despite the fact that the five stars studied here present somewhat similar spectra, and that we derived similar temperatures for them, we derived quite different helium, carbon and nitrogen abundances. The values of carbon to helium mass ratio found by us for the sample objects span a wide range of values: $0.42 < C : He < 1.96$. The case of Sand 3 seems an intriguing one. Not only we find a very low helium abundance for this star, but we also derive a high nitrogen content, when comparing these with values found in the literature for [WC] and PG1159 stars. Nitrogen abundances derived by us for the central stars of NGC 5189, Pb 6 and Sand 3 were found to be higher than previous analyses by factors of 3, 10 and 14, respectively.

By considering many elements and ionic species neglected in previous analyses, we improved the fits to the observed spectra: we were able to reproduce the observed strengths of the O V λ 1371.3 Å lines and improve the fits of the O V $\lambda\lambda$ 2781.0, 2787.0 Å lines, thanks to the consequent increase of the O V ionization fractions and we were also provided with the Ne VII λ 973 Å line diagnostic, which was modelled for the first time in [WCE] stars. The modelling of the far-UV Ne features points towards strong neon overabundances for the central stars of NGC 6905, NGC 5189, NGC 2867, and Pb 6, with Ne mass fractions between 0.01 and 0.04.

The near-UV region remains problematic: observed features both in absorption and in emission are not reproduced by our best-fitting models or grid models of any temperature and mass-loss rate and weak Ne V and Ne VI lines are predicted by the models throughout the region, but are not observed.

Acknowledgements. We thank Klaus Werner for providing many useful comments. We are also grateful to an anonymous referee for several comments that helped us improve the present paper. G.R. Keller gratefully acknowledges financial support from the Brazilian agencies CAPES (which supported her work at the Johns Hopkins University, Department of Physics and Astronomy) and FAPESP, grants 0370-09-6, 06/58240-3, and 2012/03479-2. This work was based on observations made with the Far Ultraviolet Spectroscopic Explorer, the Hubble Space Telescope, and the International Ultraviolet Explorer. The data presented in this paper were obtained from the Mikulski Archive for Space Telescopes (MAST). STScI is operated by the Association of Universities for Research in Astronomy, Inc., under NASA contract NAS5-26555. Support for MAST for non-HST data is provided by the NASA Office of Space Science via grant NNX13AC07G and by other grants and contracts. This work has made use of the computing facilities of the Laboratory of Astroinformatics (IAG/USP, NAT/Unicsul), whose purchase was made possible by the Brazilian agency FAPESP (grant 2009/54006-4) and the INCT-A.

REFERENCES

Acker, A., Marcout, J., Ochsenbein, F., Stenholm, B., Tylenda, R., Schohn, C., 1992. The Strasbourg-ESO Catalogue of Galactic Planetary Nebulae. Parts I, II.

Althaus, L. G., Córsico, A. H., Isern, J., García-Berro, E., 2010. A&A Rev., 18, 471

Althaus, L. G., Serenelli, A. M., Panei, J. A., Córsico, A. H., García-Berro, E., Scóccola, C. G., 2005. A&A, 435, 631

Barlow, M. J., Hummer, D. G., 1982. In De Loore, C. W. H., Willis, A. J., eds, Wolf-Rayet Stars: Observations, Physics, Evolution. vol. 99 of *IAU Symposium*, 387–392

Bianchi, L., Vassiliadis, E., Dopita, M., 1997. ApJ, 480, 290

Blöcker, T., 2001. Ap&SS, 275, 1

Bohlin, R., Hartig, G., 1998. Clear Aperture Fractional Transmission for Point Sources. Tech. rep.

Cahn, J. H., Kaler, J. B., Stanghellini, L., 1992. A&AS, 94, 399

Cardelli, J. A., Clayton, G. C., Mathis, J. S., 1989. ApJ, 345, 245

Crowther, P. A., Abbott, J. B., Hillier, D. J., De Marco, O., 2003. In Kwok, S., Dopita, M., Sutherland, R., eds, Planetary Nebulae: Their Evolution and Role in the Universe. ASP, vol. 209 of *IAU Symposium*, 243

Crowther, P. A., De Marco, O., Barlow, M. J., 1998. MNRAS, 296, 367

Dessart, L., Owocki, S. P., 2002. A&A, 383, 1113

Dessart, L., Owocki, S. P., 2003. A&A, 406, L1

Dessart, L., Owocki, S. P., 2005. A&A, 437, 657

Draine, B. T., Malhotra, S., 1993. ApJ, 414, 632

Feibelman, W. A., 1996a. ApJ, 472, 294

Feibelman, W. A., 1996b. ApJ, 464, 910

Górny, S. K., Tylenda, R., 2000. A&A, 362, 1008

Hamann, W. R., Koesterke, L., Wessolowski, U., 1993. A&A, 274, 397

Herald, J. E., Bianchi, L., 2002. ApJ, 580, 434

Herald, J. E., Bianchi, L., 2004a. ApJ, 609, 378

Herald, J. E., Bianchi, L., 2004b. ApJ, 611, 294

Herald, J. E., Bianchi, L., Hillier, D. J., 2005. ApJ, 627, 424

Herwig, F., 2001. Ap&SS, 275, 15

Hillier, D. J., Miller, D. L., 1998. ApJ, 496, 407

Iben, I., Jr., Kaler, J. B., Truran, J. W., Renzini, A., 1983. ApJ, 264, 605

Keller, G. R., Bianchi, L., Herald, J. E., Maciel, W. J., 2012a. In Manchado, A., Stanghellini, L., Schnberner, D., eds, Planetary Nebulae: An Eye to the Future. vol. 283 of *IAU Symposium*, 404–405

Keller, G. R., Bianchi, L., Herald, J. E., Maciel, W. J., 2012b. In Carciofi, A. C., Rivinius, T., eds, Circumstellar Dynamics at High Resolution. vol. 464 of *Astronomical Society of the Pacific Conference Series*, 309

Keller, G. R., Herald, J. E., Bianchi, L., Maciel, W. J., Bohlin, R. C., 2011. MNRAS, 418, 705

Koesterke, L., Dreizler, S., Rauch, T., 1998. A&A, 330, 1041

Koesterke, L., Hamann, W.-R., 1997a. In Habing, H. J., Lamers, H. J. G. L. M., eds, Planetary Nebulae. KLUWER, vol. 180 of *IAU Symposium*, 114

Koesterke, L., Hamann, W.-R., 1997b. A&A, 320, 91

Leuenhagen, U., Hamann, W.-R., 1998. A&A, 330, 265

Leuenhagen, U., Hamann, W.-R., Jeffery, C. S., 1996. A&A, 312, 167

Leuenhagen, U., Koesterke, L., Hamann, W.-R., 1993. Acta Astronomica, 43, 329

Maciel, W. J., 1984. A&AS, 55, 253

Marcolino, W. L. F., de Araújo, F. X., Junior, H. B. M., Duarte, E. S., 2007a. AJ, 134, 1380

Marcolino, W. L. F., Hillier, D. J., de Araujo, F. X., Pereira, C. B., 2007b. ApJ, 654, 1068

Milingo, J. B., Henry, R. B. C., Kwitter, K. B., 2002a. ApJS, 138, 285

Milingo, J. B., Kwitter, K. B., Henry, R. B. C., Cohen, R. E., 2002b. ApJS, 138, 279

Miller Bertolami, M. M., Althaus, L. G., 2006. A&A, 454, 845

Moffat, A. F. J., 2008. In Hamann, W.-R., Feldmeier, A., Oskinova, L. M., eds, Clumping in Hot-Star Winds. Potsdam univ. Press, 17

Moos, H. W., Cash, W. C., Cowie, L. L., Davidsen, A. F., Dupree, A. K., Feldman, P. D., Friedman, S. D., Green, J. C., Green, R. F., Gry, C., Hutchings, J. B., Jenkins, E. B., Linsky, J. L., Malina, R. F., Michalitsianos, A. G., Savage, B. D., Shull, J. M., Siegmund, O. H. W., Snow, T. P., Sonneborn, G., Vidal-Madjar, A., Willis, A. J., Woodgate, B. E., York, D. G., Ake, T. B., Andersson, B.-G., Andrews, J. P., Barkhouser, R. H., Bianchi, L., Blair, W. P., Brownsberger, K. R., Cha, A. N., Chayer, P., Conard, S. J., Fullerton, A. W., Gaines, G. A., Grange, R., Gummin, M. A., Hebrard, G., Kriss, G. A., Kruk, J. W., Mark, D., McCarthy, D. K., Morbey, C. L., Murowinski, R., Murphy, E. M., Oegerle, W. R., Ohl, R. G., Oliveira, C., Osterman, S. N., Sahnow, D. J., Saisse, M., Sembach, K. R., Weaver, H. A., Welsh, B. Y., Wilkinson, E., Zheng, W., 2000. ApJ, 538, L1

Oskinova, L. M., Hamann, W.-R., Feldmeier, A., 2007. A&A, 476, 1331

Peña, M., Rechy-García, J. S., García-Rojas, J., 2013. Rev. Mexicana Astron. Astrof., 49, 87

Peña, M., Stasińska, G., Medina, S., 2001. A&A, 367, 983

Rauch, T., Dreizler, S., Wolff, B., 1998. A&A, 338, 651

Schmutz, W., Hamann, W.-R., Wessolowski, U., 1989. A&A, 210, 236

Seaton, M. J., 1987. Journal of Physics B Atomic Molecular Physics, 20, 6363

Seaton, M. J., Yan, Y., Mihalas, D., Pradhan, A. K., 1994. MNRAS, 266, 805

Stanghellini, L., Shaw, R. A., Villaver, E., 2008. ApJ, 689, 194

Sundqvist, J. O., Owocki, S. P., 2013. MNRAS, 428, 1837

Todt, H., Kniazev, A. Y., Gvaramadze, V. V., Hamann, W.-R., Buckley, D., Crause, L.,

Crawford, S. M., Gulbis, A. A. S., Hettlage, C., Hooper, E., Husser, T.-O., Kotze, P., Loaring, N., Nordsieck, K. H., O'Donoghue, D., Pickering, T., Potter, S., Romero-Colmenero, E., Vaisanen, P., Williams, T., Wolf, M., 2013. MNRAS, 430, 2302

Todt, H., Peña, M., Hamann, W.-R., Gräfener, G., 2010. In Werner, K., Rauch, T., eds, American Institute of Physics Conference Series. vol. 1273, 219

Tylenda, R., Siódmiak, N., Górny, S. K., Corradi, R. L. M., Schwarz, H. E., 2003. A&A, 405, 627

Weidmann, W. A., Gamen, R., 2011. A&A, 526, A6

Werner, K., Heber, U., 1991. A&A, 247, 476

Werner, K., Herwig, F., 2006. PASP, 118, 183

Werner, K., Jahn, D., Rauch, T., Reiff, E., Herwig, F., Kruk, J. W., 2007. Baltic Astronomy, 16, 142

Werner, K., Rauch, T., Kruk, J. W., 2010. ApJ, 719, L32

Werner, K., Rauch, T., Kruk, J. W., Kurucz, R. L., 2011. A&A, 531, A146

Werner, K., Rauch, T., Reiff, E., Kruk, J. W., Napiwotzki, R., 2004. A&A, 427, 685

Appendices

A ONLINE-ONLY FIGURES

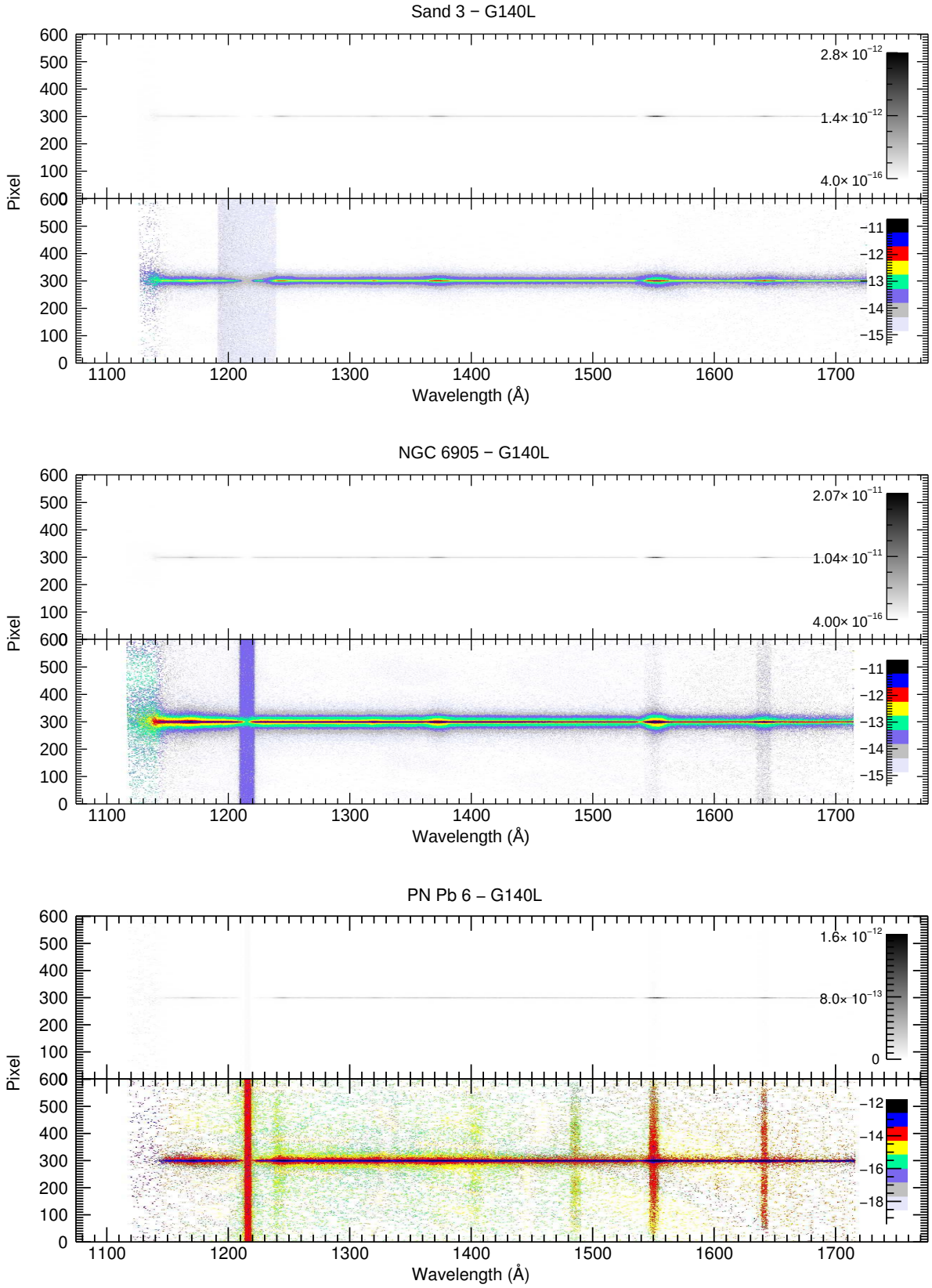

Figure 15. HST/STIS 2D Sand 3 G140L (top panel), NGC 6905 G140L (central panel), and Pb 6 G140L (bottom panel) spectra. Each spectrum is shown in linear grey scale (top) and logarithmic scale (bottom). The spatial direction comprehends 14.4 arcseconds. The vertical bands around 1216 Å are due to geocoronal Ly-α emission. The objects were observed using different slit widths, as described in Table 2.

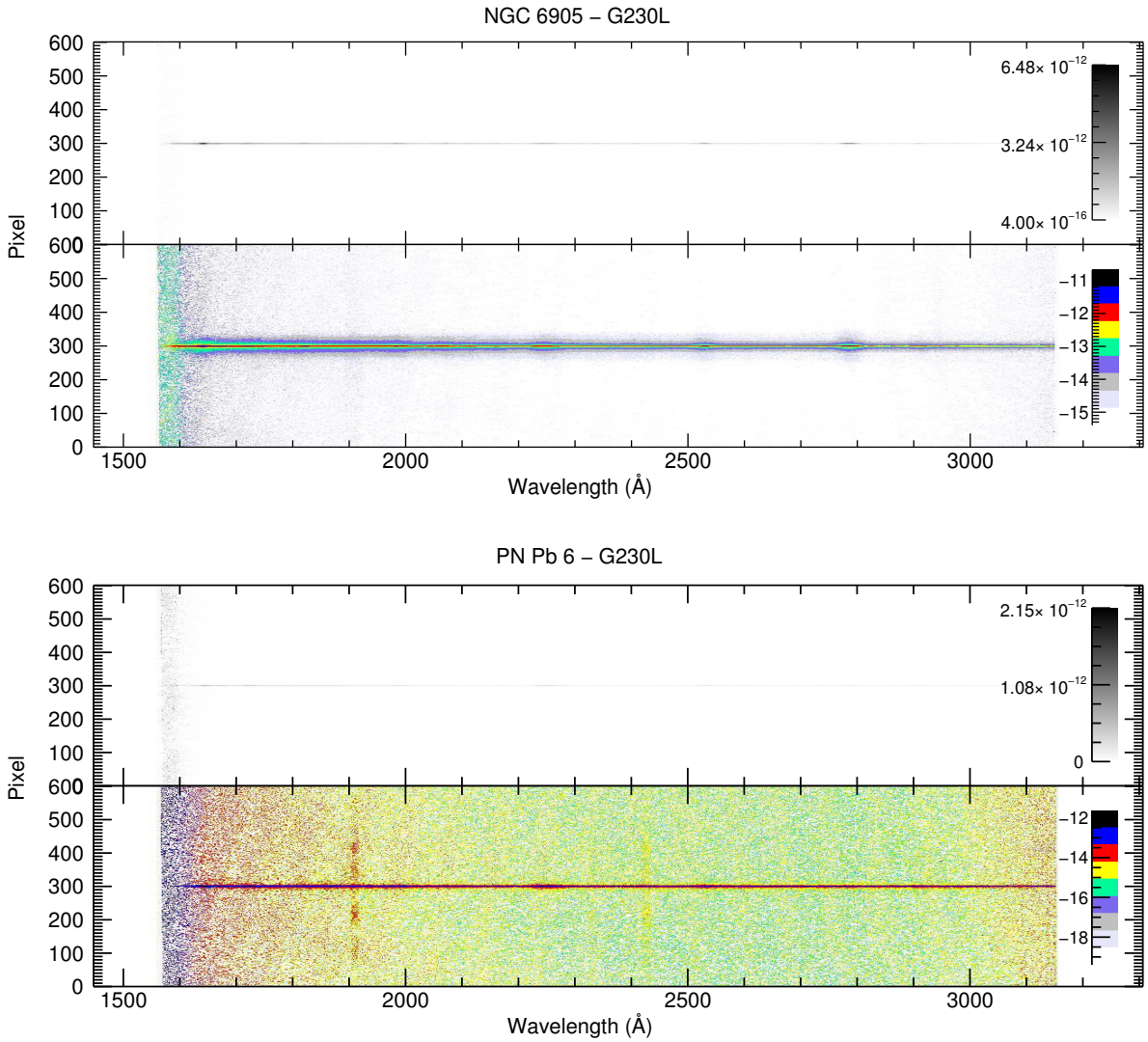

Figure 16. HST/STIS 2D NGC 6905 G230L (top panel) and Pb 6 G230L (bottom panel) spectra. Each spectrum is shown in linear grey scale (top) and logarithmic scale (bottom). The spatial direction extends for 15 arcseconds.